UNIVERSITY OF TWENTE.

Faculty of Science & Technology

Controlled deposition of gold nanoparticles on faceted $SrTiO_3$ photocatalyst particles

Berwout Heemstra

M.Sc. Thesis
January 2023

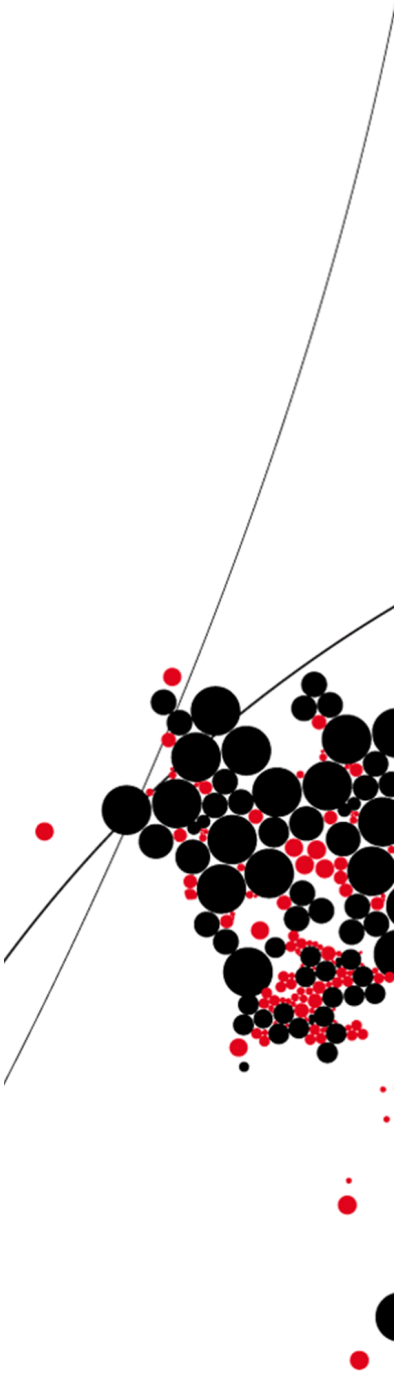

Supervisors:
Msc. Shaoqiang Su, Dr. Igor Sîretanu
Dr. Bastian Mei, Prof. Frieder Mugele

Physics of Complex Fluids group
Faculty of Science & Technology
University of Twente
P.O. Box 217
7500 AE Enschede
The Netherlands

Abstract

The hydrogen economy is expected to grow in efforts to combat climate change. This is because hydrogen is a clean fuel that can be used without producing any greenhouse gases. In the production of hydrogen, among other applications, photocatalysis could play a big role. In this process a photocatalyst needs a cocatalyst(s) in order to efficiently split water into hydrogen and oxygen. In this thesis a new method of facet-selectively depositing a gold cocatalyst onto faceted $SrTiO_3$ particles is investigated. This method uses the electrical attraction between pre-formed gold nanoparticles and the $SrTiO_3$ {100} facet as well as the electrical repulsion with the {110} facet. The stability, reproducibility and other parameters are explored, which could affect the coverage of the cocatalyst particles on the $SrTiO_3$, such as salt concentration and gold nanoparticle concentration. Additionally hotodeposition of gold onto $SrTiO_3$ was done an alternative method of depositing the cocatalyst in order to observe its coverage and control. Finally the photocatalytic activity was tested of the $SrTiO_3$ particles with colloidally deposited gold cocatalysts and of the $SrTiO_3$ particles with photodeposited cocatalysts, which was done through photocatalytic degradation of methylene blue dye.

Contents

1 Introduction **5**

2 Theoretical background **12**
2.1 Photocatalysts 12
2.2 Cocatalysts 15
2.3 Interaction forces 18
2.4 Methylene Blue dye degradation 20

3 Methods and materials **22**
3.1 $SrTiO_3$ synthesis 22
3.2 Zeta potential measurements 22
3.3 Gold colloidal deposition 23
3.4 Gold photodeposition 23
3.5 SEM imaging 24
3.6 Methylene blue photocatalytic degradation 24

4 Results **27**
4.1 Colloidal deposition of gold 30
4.2 Photodeposition 42
4.3 Photocatalytic activity 47

5 Conclusion and recommendations **52**
5.1 recommendations 52
5.2 What did I learn? 53

A Appendix **65**

1 Introduction

In order to solve the problem of climate change, a big shift towards green energy production is necessary. In this regard many renewable energy technologies are being developed, improved, scaled up and used in society, such as wind and solar energy. In the Netherlands 11.1 percent of energy consumed comes from renewable sources. [1] However this is still not enough to stop climate change. The green energy production should grow to at least 32 percent by 2030 according to a 2014 climate package for the whole European Union. [2] This means there has to be a substantial increase in the amount of renewable energy production.
Worldwide there is also a growing trend of increases in renewable energy production from 2019 to 2020 there was an almost 7% increase in electricity generation from renewables. [3] Therefore research and development into this area can be very beneficial to further expand this growth.
Photovoltaics and wind are currently the most prominent clean renewable energy sources to produce electricity. The share of electricity production from these sources accounted for just over 2% of global electricity generation for solar technologies and around 5% for wind energy technologies in 2019. [4]
These conventional renewable energy sources, such as photovoltaics and wind turbines, enable the production of large amounts of electricity that is very intermittent. This means that times of peak demand often do not match with times of peak production of electricity. Therefore additional costly installations would be required, such as batteries and electrolyzers for downstream storage and conversion to stable chemical products. [5] [6]
Hydrogen is emerging as one of the leading options for storing energy from renewables. Several advantages include that it is transportable, utilisable, and long-term storable. [7] [8] This would create possibilities of transporting the energy generated from renewables over long distances to power-hungry regions thousands of kilometers away. It can also solve the intermittency issues that is described above for photovoltaics and wind energy by bridging the gap between the energy production from renewables. Additionally it can provide more energy security and system resillience. Hydrogen can be used to supply electricity, power cars and heat homes, all with zero carbon emissions. [9]
Hydrogen has many other uses, such as producing fertilizer or oil refining or as a substitute for fossil fuels in carbon inteseive industrial processes, for instance in the steel and chemical sectors. [10] [11] [12]

There are multiple ways of producing hydrogen from water, such as thermochemical, where (waste) heat is used to drive a chemical reaction to form hydrogen, [13] electrolytic, where an electrical current is used to produce hydrogen, [14], biological, in which bacteria or algae produce hydrogen [15], and photocatalytic water splitting, where the energy from the sunlight is directly used to form hydrogen. [16]

Currently 96% of the hydrogen production is through natural gas, which means it is still not a clean energy source. [17] The share of energy produced from hydrogen in Europe is projected to grow from less than 2% to 13-14% by 2050. [18] Therefore creating more hydrogen in a renewable way is important to reduce greenhouse gases and warrants more research. [19]
Water splitting for hydrogen production using sunlight is possible through photovoltaic (PV) electrolysis or through photocatalysis. PV electrolysis uses the produced electricity from the photovoltaic cell to perform electrolysis using an anode and a cathode submerged in water. [20]
Photocatalysis on the other hand follows its natural counterpart photosynthesis and directly converts the energy from the absorbed sunlight into stable chemical products at the surface of the nanoparticle. Possible products include H_2 as a green renewable fuel, but also other fuels and base chemicals such as hydrocarbons, alcohols and ammonia. [21] Photocatalysis provide additional benefits in H_2 production, such as using a closed-loop cycle and only using incredibly abundant natural resources which are water and sunlight, with mild reaction conditions, simple setup and potential scalability. A picture, which schematically shows the process of photocatalysis can be seen in figure 1. [22] [23] [24]

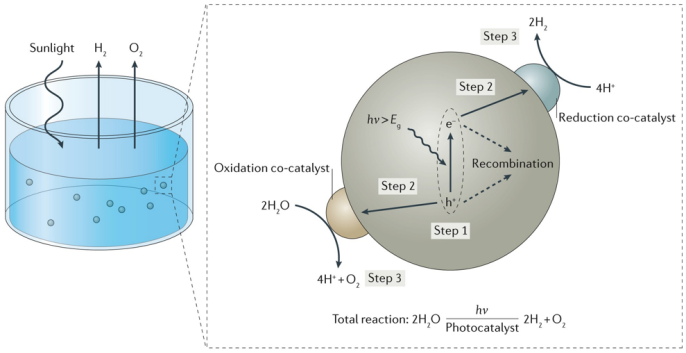

Figure 1: Schematic of photocatalytic water splitting using nanoparticles. Sunlight is absorbed by the semiconductor photocatalyst, which creates electrons and holes. These migrate to the cocatalyst at the surface, which then reduces or oxidizes the water. Adapted from Chen et al. (2017) [25]

There are a couple important factors for the material that is used in the photocatalytic process [24]: A suitable visible light absorption potential to use as much energy as possible from the sunlight. Good separation efficiency of the photogenerated holes and electrons as well as transferring them to the surface without recombination. Additionally things, such as a fast charge transfer rate to increase the reaction rate, a short energy bandgap ($<$3 eV) for the energy for the reactions, high mechanical and thermal stability, non-toxicity,

abundance, scalability and recyclability are also of importance. Hence since 1972 when Fujishima, and Honda first used the TiO_2 semiconductor photocatalyst for hydrogen production via water-splitting, a lot of effort was invested to find a material that has the above mentioned requirements. [26]

A big challenge is to find all of these aspects in one material. For instance materials such as $SrTiO_3$ and TiO_2 have a large bandgap, which does not allow much of the solar spectrum to be used for the water splitting. WO_3 has an unsuitable band position, which causes the water splitting reactions to be greatly reduced. This is because the conduction band should be more negative than the potential to reduce H^+ and the valence band should be higher than the oxidation potential of O_2 to ensure the redox reactions can happen. Other materials such as CdS or CdSe are unstable, because they suffer from corrosion from sunlight. [27] Despite the impressive progress in recent years, the ideal photocatalyst and optimum process conditions have yet to be found.

According to the current paradigm optimum performance is achieved using faceted nanoparticles (FNPs) of semiconducting materials (TiO_2, $SrTiO_3$, $BiVO_4$, WO_3 and others) that are reported to be very efficient in separation and transfer of photogenerated charge carriers (electron and holes) to surface of the particles for the desired redox reactions, such as water splitting or CO_2 reduction. The current best solar water splitting system is done through photovoltaics coupled with an electrolyser, which reaches a solar-to-hydrogen conversion efficiency of 30% in a laboratory setting. [28] Comparatively photocatalysis reaches roughly 1%, but it has a simpler, cheaper and more scalable system. [29] The current highest recorded photocatalytic hydrogen production on large scale reaches 0.76% of solar-to-hydrogen conversion efficiency by Nishiyama et al.(2021) [30] Al-doped $SrTiO_3$ photocatalyst sheets were used for the water splitting loaded with Rh, Cr, and Co, all at 0.1 wt%. This system was optimized for safety and durability, although there are still many optimizations to be done. [30]

This is, however, still far from commonly accepted industrial requirements for large-scale applications (efficiency of 5–10% and system lifetime of 5 years). [31]

An important aspect that has to be considered for high solar-to-hydrogen (STH) efficiency is using the right cocatalyst metal or metal-oxide at the right place on the photocatalyst, since the photocatalytic activity of bare semiconductors particles is extremely low. Loading a metal or metal-oxide cocatalyst onto a semiconductor photocatalyst lowers the overpotential/energy barrier for the hydrogen and oxygen evolution reactions and hence increases the photocatalytic activity. [32] For instance bare $BiVO_4$ loaded with Pt and MnO_x increases the oxygen evolution amount around 800 times as compared to bare $BiVO_4$ particles. [23] Additionally loading Pt and Co_3O_4 facet selectively using photodeposition increases the water splitting by up to 10 times compared to deposition using impregnation. [33]

Figure 2 shows a volcano plot of the hydrogen evolution rate expressed as exchange current against the adsorption energy expressed as metal-hydrogen bond strength. From the plot we can see that the highest exchange current, and thus the highest hydrogen

evolution rate, is found at the top of the volcano, where the adsorption energy is in the middle.
Sabatier's principle suggested this, which is the idea that the absorption energy should not be too high nor too low. If the adsorption energy is too high the adsorption is slow and if the adsorption energy is too low the desorption is slow. So there is an optimum to balance the adsorption and desorption time to allow for the most throughput in terms of reactions taking place. [34] [35]
From figure 2 we can see that the top of the volcano has traditional catalytic materials like platinum or rhodium. Here we will use gold as a cocatalyst, since it also has reasonable performance and gold colloidal nanoparticles with controlled shape and size are available. Moreover the photocatalytic activity of semiconductor materials is also affected by the size of the cocatalyst, their coverage and distribution, particle morphology and shape, chemical composition, oxidation state and the properties of the interface between the metal cocatalyst and the semiconductor particle. [36] For instance the rate of hydrogen production increases 3 fold if the size of the ruthinium cocatalyst particles is varied from 1.5 nm instead of 7 nm. [37] The hydrogen evolution rate increases 2-3 times if tetrahedral palladium particles are used instead of cubes on TiO_2. [38]

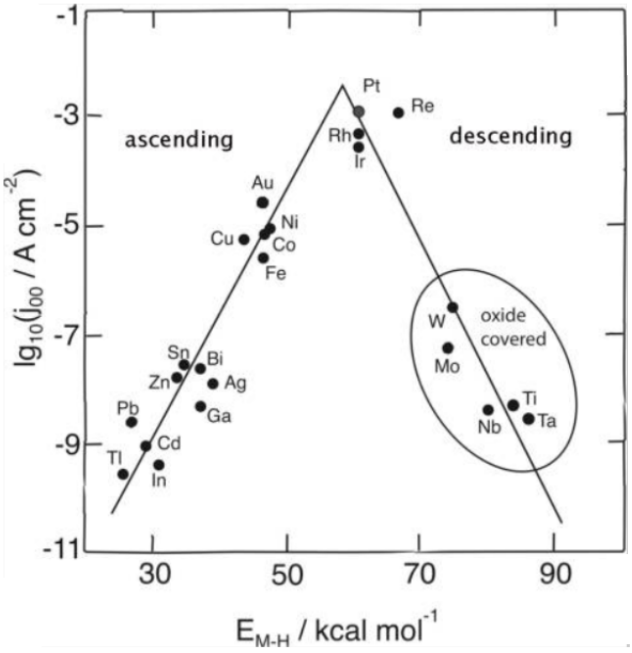

Figure 2: Plot of the log of the exchange current for hydrogen evolution against the energy of the metal-hydrogen bond. Adapted from Trasatti (1972). [35]

The most common ways to deposit cocatalysts onto the photocatalyst are through im-

pregnation or photodeposition. A scematic of the difference between impregnation and photodeposition are shown in figure 3. Impregnation is generally done by submerging the powder of photocatalytic particles in a metal or metal-oxide precursor and subsequently drying and annealing at high temperature. This is a fairly simple procedure although randomly distributed over the photocatalyst. [22]
Photodeposition is usually done through mixing the photocatalyst with a metal or metal-oxide precursor ions and subsequent illumination. This illumination causes an electrochemical reduction or oxidation reaction to take place which deposits the metal or metal-oxide onto the photocatalyst, through the reduction or oxidation of the precursor. This results in a photocatalyst decorated with cocatalyst nanoparticles at the location (or facet) where the electrons reach the surface. [39]

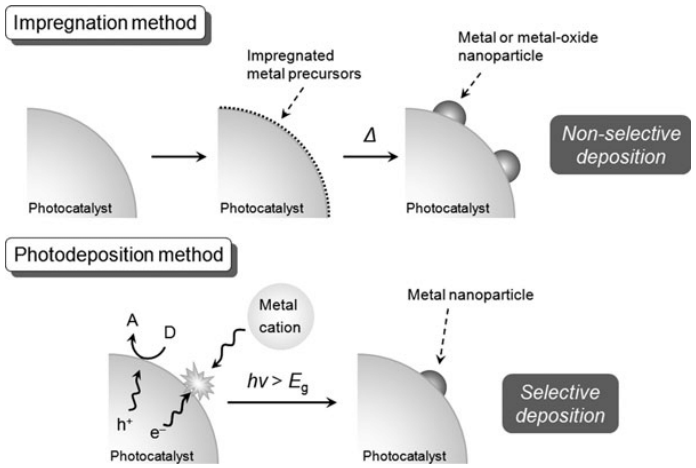

Figure 3: Schematic illustration of impregnation and photodeposition as a method of depositing cocatalysts. Adapted from Carraro et al. (2011) [40]

Yet, neither of these two processes allow good control on the above mentioned crucial aspects like cocatalyst size, particle morphology, loading and distribution, etc. [36] Additionally, during (initial stages of) the catalytic process the cocatalyst particles rearrange and relocate, dissolve and change their physiochemical properties (oxidation state and phase composition) drastically reducing the semiconductor-cocatalysts material properties. In figure 4 this rearrangement of Ni and NiO_x cocatalysts on $SrTiO_3$ can be seen, which leads to a decrease in overall water splitting over time. [41]
Deposition of cocatalyst (metal/metal oxide) on faceted nanoparticles using pre-synthesized colloidal nanoparticles may give better control on the process in terms of the amount of cocatalyst that is deposited, their distribution on individual facets of semiconductor nanoparticles, the size (and shape) of the cocatalyst particles, oxidation state and cocatalysts particle stability during the photocatalytic process. This could potentially give rise to a better photocatalytic performance and stability of the materials. Currently metal and

metal oxide nanocrystals with well-defined size, shape, oxidation state, exposed facets and stability can be easily prepared via colloidal synthesis. [42] [43]

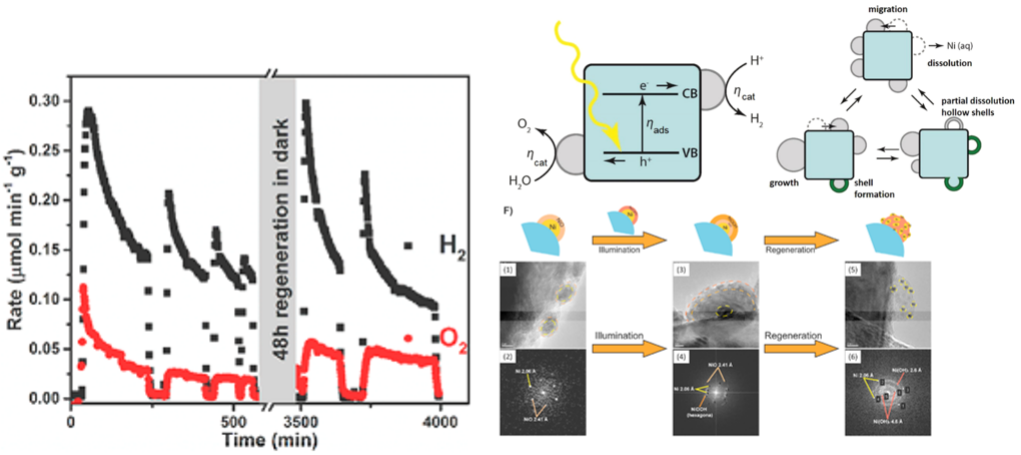

Figure 4: The left picture shows the hydrogen evolution rate as a function of time. The top right shows a schematic of the processes involved during illumination of photodeposited cocatalysts. The bottom right shows changes in morphology of NiO_x on Ni on $SrTiO_3$ during overall water splitting. Adapted from Mei et al. (2018) [41]

There are several ways to test the photocatalytic activity of these photocatalysts, such as hydrogen evolution tests or photocatalytic dye degradation. [33] [44] The most common method of assessing the water splitting capability of a photocatalyst is by measuring the gases produced by a water splitting or hydrogen evolution test using gas chromatography or mass spectrometry. [22] Another straightforward alternative is dye degradation method, in which a dye such as methylene blue (MB) is degraded to H_2O and CO_2 through photocatalysis processes. [45] Dye degradation by itself has the purpose of removing toxic industrial dyes to provide clean drinking water, which helps lead to a more livable and safe world. [45] Additionally there are some other ways such as air purification and biorefinery, which are rarely used. [46] [21]
The research goals of this thesis are twofold; firstly, test if gold cocatalysts nanoparticles can be adsorbed selectively onto individual facets of onto SrTiO3 nanocrystals. Establish the working protocol for this process. Assess if the gold nanoparticle coverage is affected and can be controlled by the NaCl ion concentration, pH of the solution or the concentration of gold nanoparticles solution that is added. Secondly, test the photocatalytic activity of the $SrTiO_3$ with gold colloidal nanoparticles as cocatalyst and assess if there is an improvement compared to $SrTiO_3$ particles loaded with cocatalysts via the commonly used method, i.e. through photodeposition. [22] The inspiration for this project is based on

work by Su et al. [47] who showed that it is possible to facet-selectively deposit silica nanopartilces onto faceted $SrTiO_3$.

2 Theoretical background

There are three main steps to photocatalytic water splitting: [48]

1. Harvesting as much sunlight as possible with the semiconductor photocatalyst to create electron-hole pairs.
2. Separating the electrons and holes and migrating to the surface, without recombining.
3. Finally the reducing and oxidizing of the water at the surface of the photocatalyst as efficiently as possible to create H_2 and O_2.

To optimize each part of the water splitting process, it is important to address each point to find improvements in these areas.

2.1 Photocatalysts

$SrTiO_3$ is used as a semiconductor as a means of harvesting sunlight in this thesis. This is because of the appropriate band gap, non-toxicity and the stability of the material as well as the ability to engineer the facets of the particles. [49] [33] Although there are alternatives to be considered.
One of the oldest semiconductors that is used is for water splitting is TiO_2 as early as 1972. [26] TiO_2 is a photocatalyst with a band gap of 3.2 eV and it has been studied because of its high stability, low cost and non-toxicity. [50] Although a problem is that TiO_2 has a wide band gap, which limits its ability to absorb light in the visible spectrum. To decrease the band gap it could be possible to couple TiO_2 with a visible light semiconductor, such as ZnO, which might enhance the photocatalytic activity. [51]
Among the visible light semiconductors are graphic carbon nitride (g-C_3N_4), which is a low cost, metal-free polymeric photocatalyst. [52] It has a lower band gap and appropriate band structure at 2.7 eV, while also having high thermal and chemical stability. Although its limtations are its low surface area, small active sites for interfacial reactions and low charge mobility. Coupling and/or doping g-C_3N_4 with other elements could ameliorate these limitations.
$BiVO_4$ is another potential candidate as a photocatalyst with a big advantage of having a smaller bandgap at 2.4 eV, which allows it to capture more of the sunlight. Some disadvantages, however, include low electron conductivity and poor water oxidation kinetics, as well as limited stability. [53] Coupling is a way of increasing photocatalytic activity by forming contact between two different semiconductor particles, which can be done in similar ways as cocatalyst deposition. [54] $BiVO_4$ coupled with other semiconductor materials shows an improvement in photocatalytic activity, which is attributed to increased charge separation. [55]

These materials might be improved by doping or coupling, where coupling is usually done by forming contact with other semiconductors, and doping is usually done by inserting metal atoms into the semiconductor, but organic materials are possible as well. [56] Doping of a semiconductor is usually done by some form of calcination or heat treatment with metal precursor, which causes the metal atoms to insert into the semiconductor. [57] This is generally done to attempt to improve some aspect of the photocatalyst, such as reducing the size of the wide band gap of $SrTiO_3$. For instance doping using transition metals such as rhodium or aluminum shows reduction in the band gap and increases in photocatalytic activity. [58]
$SrTiO_3$ is a semiconductor with a cubic perovskite structure, which is typically produced as cubic-shaped nanoparticles with 6 identical {100} facets. Due to it having identical facets it is difficult to spatially separate the electrons and holes. It is possible to produce the $SrTiO_3$ particles, such that both the {100} and the {110} surfaces are exposed. This way, the particles can be produced with 18 flat facets, such as can be seen in figure 5. [33] [59] This anisotropy of the $SrTiO_3$ particles increases the charge separation in the particle, which is attributed to an internal electric field, which drives the electrons and holes to different facets, which can be observed in figure 6. This electric field is in turn attributed to the difference in surface potential, which originates from the different surface orientation of the different facets. As can be seen from simulations from Takata et al.(2020) [29] in figure 6, this difference in surface work function causes the electrons and holes to collect at the {100} and {110} facet respectively. So this anisotropy increases charge separation, which is shown to increase photocatalytic activity. [29] [60] [33]

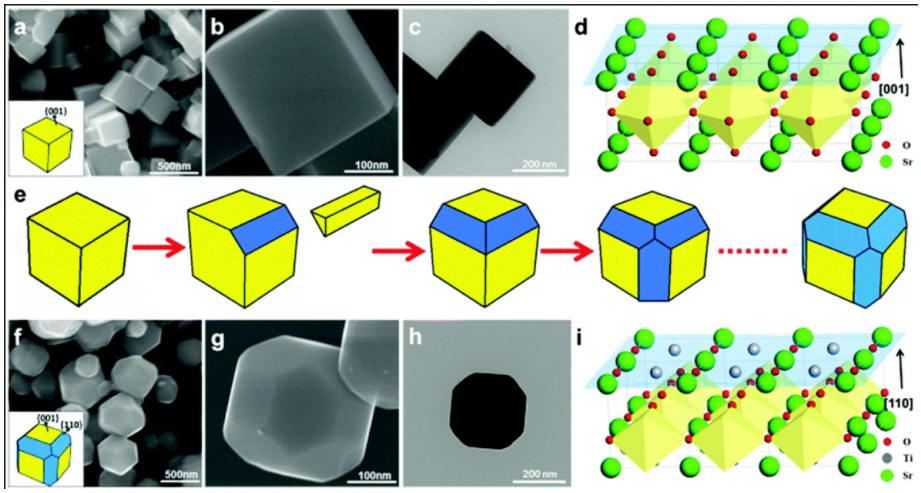

Figure 5: (a-c) The morphology of isotropic 6-facet $SrTiO_3$ particles. (d) structure of the 100 facet of $SrTiO_3$. (e) Schematic of facet engineering of $SrTiO_3$. (f-h) The morphology of the anisotropic 18-facet $SrTiO_3$ particles. (i) the structure of the 110 facet of $SrTiO_3$. adapted from Mu et al. (2016) [33]

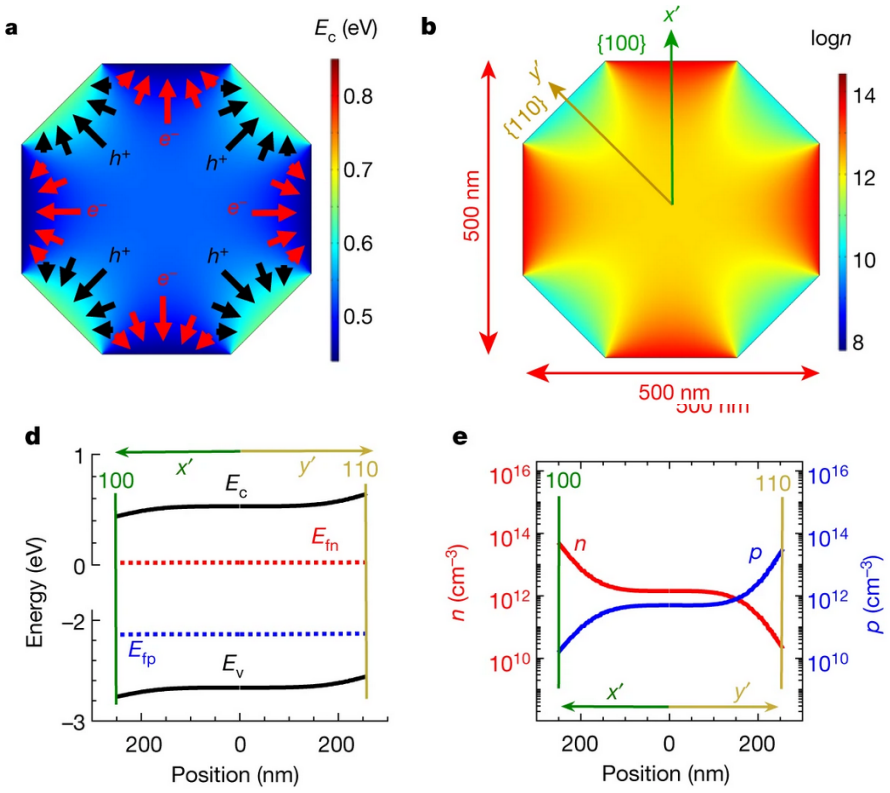

Figure 6: Simulations of electrons and holes in aluminum doped $SrTiO_3$ particles. (a) Mapping of conduction band energy, (b) Colourmap of the density of electrons n, (d) diagram of energy of conduction and valence band when approaching different facets, (e) electron and hole densities approaching different facets. adapted from Takata et al. (2020) [29]

2.2 Cocatalysts

Water splitting is an energetically uphill reaction ($\Delta G^{\ominus}$ = 237 kJ/mol, which is equal to 1.23 eV). It produces hydrogen and oxygen in a 2:1 ratio, which means two water molecules have to be split in order to complete one reaction as shown in equations 1 - 3. This requires the transfer of four electrons, namely two to oxidize the water and two to reduce the hydrogen ions. [22]

$$4h^+ + 2H_2O \rightarrow O_2 + 4H^+ (\text{oxidation of water}) \quad (1)$$

$$2e^- + 2H^+ \rightarrow H_2 (\text{proton reduction}) \quad (2)$$

$$2H_2O + 4h^+ + 4e^- \rightarrow 2H_2 + O_2 (\text{overall water splitting}) \quad (3)$$

Cocatalyst particles can be deposited, or loaded, onto the semiconductor photocatalyst to increase the photocatalytic activity. These cocatalysts can serve as reaction sites for water splitting and help in this process by lowering the activation energy required for the redox reaction as well as enhancing charge separation. [22]

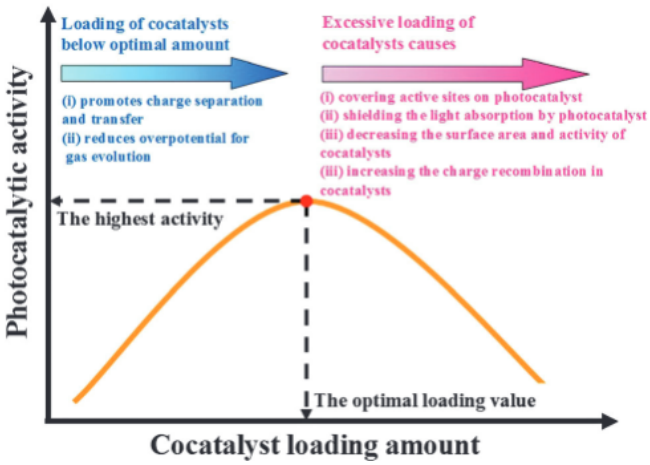

Figure 7: Volcanoplot of photocatalytic activity against cocatalyst loading amount. Adapted from Ran et al.(2014) [61]

A volcano type relationship is shown in figure 7, which illustrates that for any photocatalyst and cocatalyst system a certain optimal loading of the cocatalyst can be reached. This is a balance between different factors. For instance the photocatalytic activity increases, while the loading increases, because it increases charge separation and helps to overcome the energy barrier for water splitting. However when too much of the cocatalyst is deposited, it can block the photocatalyst from incoming light, which prevents the absorption of photos and thus the generation of electron-hole pairs. It can also decrease the usable surface area of other cocatalysts on the semiconductor, among other possible reasons. [61]

There are several ways of depositing cocatalysts, such as commonly through impregnation or photodeposition, although other methods have been tried as well, such as sputtering. [33] [62] Of these methods photodeposition is considered the best option as this allows for facet selective deposition, which greatly increases the charge separation. This reduces recombination of the electrons and holes and therefore the photocatalytic performance. [22]

Photodeposition is done through illumination of the photocatalyst in metal precursor solution. This illumination causes an electrochemical reduction or oxidation reaction to take place which deposits the metal or metal-oxide onto the photocatalyst. These reactions can

be seen in equations 14 15, where M stands for metal and MO stands for metal-oxide, n is an integer and e and h are electrons and holes respectively. [39]

$$M^{n+}(aq) + ne^- \rightarrow M(s) \tag{4}$$

$$M^{n+}(aq) + nh^+ + nH_2O \rightarrow MO_n(s) + 2nH^+ \tag{5}$$

Due to the fact that electrons and holes are used in these reactions, combined with the fact that the electrons and holes are separated to different facets makes this a facet selective method of cocatalyst deposition. This in turn improves the charge separation and improves photocatalytic activity. [33]
Because they are reduction or oxidation reactions, in some cases an electron or hole scavenger is added respectively, such as H_2O_2 or CH_3OH. These can improve the reduction or oxidation reactions by acting as a hole or electron acceptor respectively. This improves the reaction by taking or providing an electron to reduce or oxidize the second part of the redox reaction. [63]
Typical scanning electron microscopy (SEM) images of impregnation and photodeposition of platinum cocatalyst onto faceted $SrTiO_3$ by Mu et al. (2016) are shown in figure 8. In the first image the Pt cocatalyst is deposited quite homogeneously all over the $SrTiO_3$ particle regardless of the facet. On the other hand the Pt cocatalyst is selectively deposited onto the square $\{100\}$ facet, while a MnO_x cocatalyst is also deposited onto the $\{110\}$ facet. Even though the deposition is facet selective, the distribution on the facet is not very homogeneous. [33]

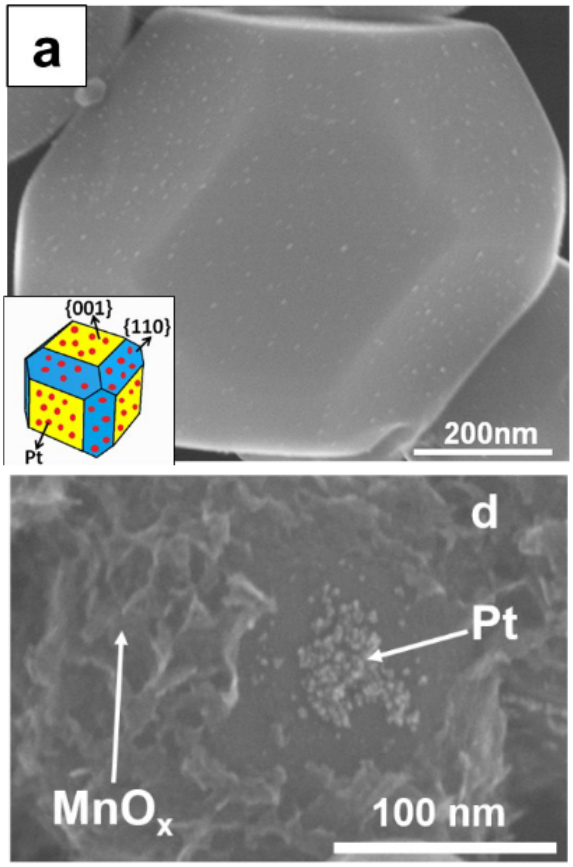

Figure 8: SEM images of cocatalyst deposition on anisotropic $SrTiO_3$ particles using impregnation of (top) and photodeposition of Pt and MnO_x (bottom). Adapted from Mu et al. (2016). [33]

2.3 Interaction forces

Upon interaction of small gold nanoparticles and another colloid or particle, such as faceted $SrTiO_3$, the following forces should be considered. First is the electrical double layer force. The second is the VanderWaals force. The third one is short range hydration forces. A combination of electrical double layer force and VanderWaals forces are called DLVO forces.
DLVO theory developed by Derjaguin, Landau, Verwey and Overbeek in the 1940s gives insight into the stability of colloids and the relevant forces, which is important to understand how the gold nanoparticles and $SrTiO_3$ interact. [64] [65]
VanderWaals forces originate from induced dipoles in materials when they approach each other and are almost always attractive. This force is not dependent on the salt concentra-

tion or ionic strength of the solution, in contrast to the electric double layer force. The VanderWaals force generally acts at very short distances from around 0.2 nm up to around 10 nm depending on the materials, which decays very fast with distance at a rate of $\frac{1}{r^6}$. [66] This could play a role when the gold nanoparticles stick to the surface of the $SrTiO_3$.
A particle in a liquid will get charged. This surface charge can have multiple origins. Firstly some surface groups can dissociate, such as sulfates, carboxyl, hydroxyl and oxides, which will have a charge. Dissolution of an ion from the surface of the colloid into the liquid, which can cause the surface of the solid to gain or lose a charge. Charged ions can also be specifically adsorbed onto the surface, which will also change the surface charge. [67]
This surface charge is usually screened by ions in the liquid to achieve overall electrical neutrality. This screening of ions causes the formation of the electrical double layer as shown in figure 9. The Zeta potential is defined as the potential at the slipping plane as seen in the figure 9. A schematic of this electrical double layer is shown in figure 9. Here it can be seen that the negative charge at the surface of a particle is screened by particles on the Stern layer, which are very tightly bound, then the slipping plane screens those charges again, at the end of which the zeta potential is measured. Depending on the charge/potential and associated electrical double layer, the two interacting particles can attract or repel each other in the suspension. [66]
The length of this electrical double layer and the extent to which it extends into the bulk solution is controlled by the screening of this charge, through the concentration of the ions in the solution. This effect will be reduced for a lower Debye length, which is a measure for how far the electrostatic effect persists in a suspension. This Debye Length is influenced by the salt concentration of the suspension, because of the screening caused by the ions. Typically this force acts up to a few tens of nms, decreasing with an increase in salt concentration. [68] When considering deposition of the cocatalyst onto the $SrTiO_3$, The gold nanoparticles are charged, so they will electrically repel each other and interact with the charge of the $SrTiO_3$ particle.
Additionally, another force that might play a role is the hydration force, which is the force that arises from the arrangement of water molecules very close to the surface of a colloid. This is a very short range force up to 1.5 nm from the surface, which starts out as strong very close to the surface, while it propagates farther than the first row of water molecules, although increasingly more weakly as the distance increases. [68]
Specifically with regards to the faceted $SrTiO_3$ particles, Su et al (2021) have shown that the (in this case) repulsive hydration force on the {100} facet is stronger and more long range than at the {110} facet. [47] By Dong et al. (2014) it was demonstrated that $SrTiO_3$ facets surface hydration structure controls he facet-specific assembly of proteins, such as albumin, immunoglobulin and protamine. The protein adsorption was observed on weakly hydrated {100} facets of $SrTiO_3$ nanoparticles, while none on {110} facets. [69]

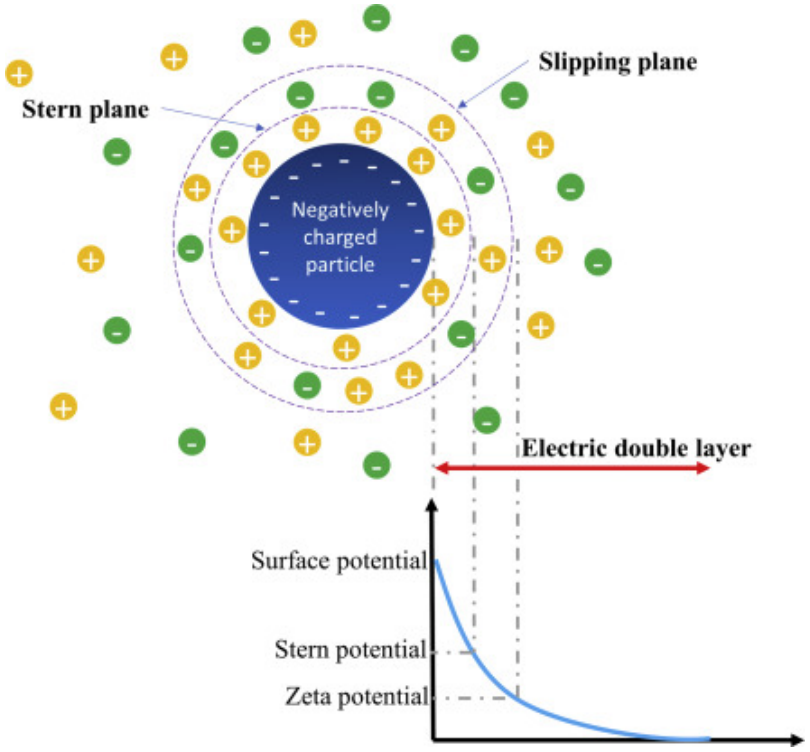

Figure 9: Illustration of the surface charge of a particle, showing the electrical double layer. Taken from Feng et al. (2020) [70]

2.4 Methylene Blue dye degradation

Photocatalytic degradation of methylene blue involves using photocatalyst particles and light in order to degrade the methylene blue particles into harmless particles such as CO_2, H_2O, $SO_4{}^{2-}$ and $NH_4{}^{+}$.

The postulated mechanism is that $O_2{}^{-}$ and OH radicals cause the degradation of the methylene blue by oxidizing and breaking up the methylene blue molecule. [71] [45] The holes and electrons that are created reach the surface. The holes can oxidize the H_2O to form OH radicals and they can attack the methylene blue molecule in order to degrade it to a colourless form, which is shown in equation 11. Additionally the holes can oxidize the methylene blue directly when it is adsorbed on the surface as shown in equation 12. [71] The electron pathway is more complicated as it involves multiple steps, which are shown in equations 7 to 10. Firstly an oxygen molecule is reduced to a radical by an electron from the photocatalyst. Subsequently the oxygen radical reacts with hydrogen ions in the solution, which then in the next step form hydrogen peroxide and oxygen. Finally the hydrogen peroxide is reduced by the photocatalyst, so that there is another OH radical

that can attack the methylene blue in order to degrade it. [71]

$$(H_2O \leftrightarrow H^+ + OH^-) + h^+ \rightarrow H^+ + OH^{\cdot} \tag{6}$$

$$O_2 + e^- \rightarrow O_2^{\cdot -} \tag{7}$$

$$O_2^{\cdot -} + H^+ \rightarrow HO_2^{\cdot} \tag{8}$$

$$2HO_2^{\cdot} \rightarrow H_2O_2 + O_2 \tag{9}$$

$$H_2O_2 + e^- \rightarrow OH^{\cdot} + OH^- \tag{10}$$

$$MB + OH^{\cdot} \rightarrow MB' + H_2O \tag{11}$$

$$MB + h^+ \rightarrow MB^* \tag{12}$$

In the equations above h^+ and e^- stand for the electrons and holes generated by the photocatalyst. The $\cdot$ superscript means it is a radical and finally MB stands for the methylene blue molecule with MB$'$ and MB* meaning reduced forms of methylene blue.

3 Methods and materials

3.1 $SrTiO_3$ synthesis

It is possible to tune the morphology of the $SrTiO_3$ as described by Dong et al. (2014) as well as Hsieh et al. (2019) , who manage to use different concentrations or pKa values of alcohols to tune the ratio of the size of the {110} facets to that of the {100} facets. [69] [60] Hsieh et al. (2019) also show that these anisotropically faceted $SrTiO_3$ particles show higher photocatalytic activity than cubic $SrTiO_3$ particles. [60] In order to create truncated dodecahedron-shaped SrTiO3 submicron particles, the procedure described by Dong et al. (2014) is followed. [69]
Firstly 3 mL 1,3-propanediol or 4 g of 1,2-propanediol is mixed with 25 mL DI water in an ice bath for 15 to 30 min while stirring. Next 0.265 mL of $TiCl_4$ was added dropwise and continuously stirred for 5 min. 30 mL of 3M LiOH solution and 10 mL of 0.24 M $SrCl_2$ solution were then added after each other. The solution was then kept stirring for 30 min. This solution was transferred to a 100 mL Teflon-lined stainless-steel autoclave, which was closed shut tightly and heated for 48 h at 180 deg C. The resulting precipitate was centrifuged and washed alternately with water and ethanol five times each, in order to clean the $SrTiO_3$ particles using a centrifuge speed of 2000 RCF for 10 min. Lastly to obtain the $SrTiO_3$ particles in powder form, they were dried at 70 degC for 12h.

3.2 Zeta potential measurements

In order to characterize the surface charge of the $SrTiO_3$ particles as well as that of the gold nanoparticles, zeta potential measurements were done at different pH values.
These measurements are done using a Zetasizer nano ZS from Malvern Panalytical. The principle that is used to measure the zeta potential is phase analysis light scattering (PALS) which uses the phase information from the light that is scattered of the particles that are moving through electrophoresis due to an applied electric field. This measures the electrokinetic potential of the particles, which is used to calculate the zeta potential. Finally the output that is obtained from the machine is the zeta potential in mV. [72]
To measure the $SrTiO_3$ particles, a solution of 40 mL 10 mM NaCl is prepared, to which 2 mg of $SrTiO_3$ is added. This solution was brought to a pH of around 9.5 using a NaOH solution, at which point a sample of 4 mL was taken and put in a cup for use in the Zetasizer. Subsequently the pH was reduced with increments of around 1 using an HCl solution, while at every increment a sample of approximately 4 mL was taken. Immediately after these samples were analysed in the Zetasizer using a cell, which was rinsed multiple times with DI water in between measurements.
The same procedure is used for the gold nanoparticles, which were measured in their citrate buffer at a concentration of approximately 0.44 mg/mL, which translates to a volume

fraction of $2.88 \cdot 10^{-6}$ of gold. 10 mL of the gold nanoparticle solution is then pH adjusted in the same way from around 9.5 to around 1.5, with samples of 1 mL taken at every increment of pH units of 1.

3.3 Gold colloidal deposition

In a typical deposition experiment of gold colloidal nanoparticles onto faceted $SrTiO_3$ particles, the following procedure was used.
Firstly a salt solution was prepared at 100 mM NaCl in 100 mL of deionized (DI) water by adding 0.5844 g of NaCl into 100 mL of DI water. This was then diluted 100 times with DI water so that a 100 mL 1 mM NaCl solution was made so that the electrical double layer force is established. Of this solution 20 mL was taken. Subsequently 2 mg of $SrTiO_3$ was weighed on an analytical balance and added to the 20 mL 1 mM NaCl solution. This solution was then placed in a sonicator for roughly 10 minutes in order to suspend the $SrTiO_3$ particles in the solution and separate them from each other so that the facets are free for the gold nanoparticles to deposit onto.
This suspension was then continuously stirred while measuring and adjusting the pH in real time. After this 3 mL of 0.44 mg/mL or 2commercial citrate-functionalised gold nanoparticles dispersed in citrate buffer with a diameter of 15 nm were added to the suspension using a pipet. The pH was then adjusted as soon as possible after adding the gold nanoparticles to its desired value (typically 3). The pH was adjusted using HCl or NaOH solutions.
The susspension was left stirring for 10 min so that the gold nanoparticles have enough mixing time to deposit onto the $SrTiO_3$. Afterwards the suspension was moved to a different container suitable for centrifuging, after which the suspension was centrifuged at 2000 RCF for 15 min. Subsequently about 90% of the solution was poured out and refilled with DI water. Then the solution was resuspended using a sonicator. This process of centrifuging and replacing the liquid is used to wash the particles by removing any excess gold nanoparticles or other contaminations and it is repeated twice more. Depending on the experiment some variables such as a pH, different salt or gold concentration were changed, these variables are specified in the results section in the figure's caption.
All chemicals used were purchased from Sigma Aldrich.

3.4 Gold photodeposition

In a typical photodeposition experiment of gold, the following procedure was used.
An appropriate amount of $HAuCl_4$ solution (4.55 mg/mL) was added to a solution of 2 mg of $SrTiO_3$ nanoparticles in 20 mL DI water. Specifically adding 0.44 μL, 8.80 μL or 22.0 μL to obtain 0.1, 2 or 5 wt% of $HAuCl_4$ respectively. Note this is a weight percentage with regards to the weight of the $SrTiO_3$ particles. The pH was then adjusted to its desired value by adding NaOH or HCl solutions. This suspension of $SrTiO_3$ particles was then

placed in a glass vial and illuminated in UV light under continuous stirring for 2 or 4 hours. The specific wavelength spectrum can be seen in figure 11.
The solution was centrifuged at 2000 RCF for 15 min. Subsequently about 90% of the solution was poured out and refilled with DI water. Then the solution was resuspended using an ultrasonic bath. This process of centrifuging and replacing the liquid is used to wash the particles and it is repeated twice more.
Depending on the experiment some variables such as a pH, methanol use or precursor ion concentration were changed, these variables are specified in the results section in the figure's caption. All chemicals used were purchased from Sigma Aldrich.

3.5 SEM imaging

Scanning electron microscopy (SEM) was used to visualize the deposition of gold nanoparticles on $SrTiO_3$. SEM works by firing an electron beam in vacuum at a sample, which then scatters electrons from the surface of the sample. These scattered electrons or even x-rays, are then caught by a detector and based on this a picture is constructed and shown on a computer screen. [73]
Energy selective backscattered (ESB) mode, is a mode which shows different levels of brightness of different materials based on their atomic numbers, this is due to the fact that an increasing amount of electrons get backscattered as the atomic number increases. The InLens mode, on the other hand, creates a picture of the sample, based on the electrons that scatter off the surface of the sample, which allows a cleared picture of its surface topology. [73]
SEM imaging of the $SrTiO_3$ particles was done by Mark Smithers at the MESA+ Nanolab. For this the particles were prepared by pipetting roughly 50 to 100 μL of the suspension of $SrTiO_3$ in DI water onto a silicon wafer, which was then dried at around 100 °C for about two minutes. Then the samples was taken to the MESA+ Nanolab and analysed in the SEM.

3.6 Methylene blue photocatalytic degradation

In order to do the dye degradation, a suspension of 10 mg of gold-decorated $SrTiO_3$ was prepared, using either photodeposition method or colloidal gold deposition method as outlined above in 100 mL of DI water. This solution was then centrifuged and the excess water removed, after which it was resuspended using the sonicator so that only 10 mL of suspension was left, which results in a concentration of 10 mg gold-decorated $SrTiO_3$ per 10 mL of water.
Additionally a methylene blue solution was prepared at 20 ppm or 20 mg/L by weighing 10 mg methylene blue powder and dissolving this in 100 mL DI water and diluting it 5 times. 10 mL of this methylene blue solution was added to a glass vial of roughly 25 mL volume. After this the 10 mL $SrTiO_3$ suspension was added into the methylene blue so-

lution so that a concentration of 10 mg/L of methylene blue was achieved with 10 mg of $SrTiO_3$ in a 20 mL solution.
The suspension was kept stirring in the dark for up to 24 hours, so that the adsorption of methylene blue to the walls of the vial and to the $SrTiO_3$ particles reaches an equilibrium. At this point the concentration of methylene blue is measured in a UV-vis photospectrometer. This is done so that the observed decline in concentration of methylene blue under illumination is due to photodegradation instead of due to any adsorption.
To analyse the concentration 2 mL of the suspension was taken. This was then placed in a container suitable for centrifuging, which was centrifuged at 2000 RCF for 10 min in order to get the $SrTiO_3$ particles out of the solution. Then 1.5 mL of the solution was taken using a pipet and placed in a different container so it is usable for use in a cuvette for the UV-vis photospectrometer. This is done so that only the methylene blue is analysed, without the $SrTiO_3$ particles. After analysing the solution, the methylene blue was placed back into the previous container with the leftover $SrTiO_3$ particles, which is then resuspended and replaced into the original suspension of $SrTiO_3$ in methylene blue in the glass vial. These steps are taken so that (practically) none of the $SrTiO_3$ particle suspension is lost during the dye degradation process.
This solution of methylene blue with $SrTiO_3$ was then illuminated under UV light for 1 hour. UV light with a spectrum of 350 to 400 nm was chosen, because the $SrTiO_3$ is able to absorb light up until about 388 nm and to minimize any photolysis of the methylene blue that is not caused by the photocatalyst. [33] [74] A picture of the setup is included in figure 10. In order to do the dye degradation, the glass vials were taped down to the stirring plate to prevent falling over and a glass cap was used to allow more light more light to reach the sample, because it was illuminated from above.
After illumination for 1 hour, 2 mL of the suspension was again taken and the process was repeated to analyse the methylene blue absorbance spectrum in the UV-vis photospectrometer.
After the analysed sample is placed back in the orginal suspension, the glass vial is placed back under illumination for another hour. This whole process was repeated until 7 hours of illumination had passed, which resulted in roughly 80-90% of the dye being degraded.

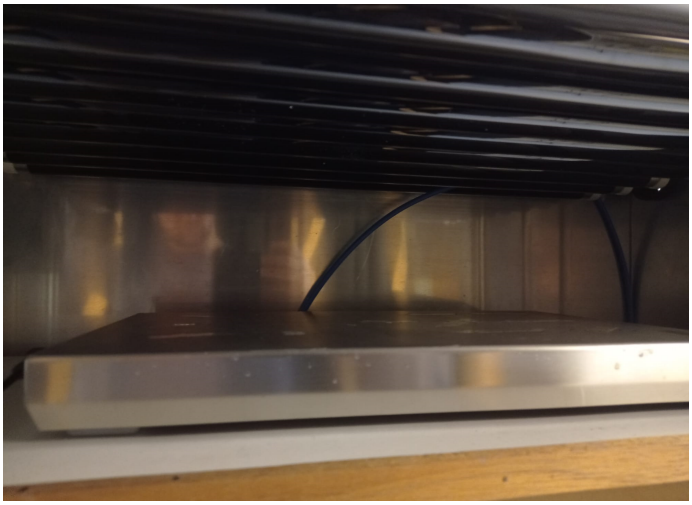

Figure 10: Picture of the setup used for illumination of samples using UV light. A row of 8 lamps of 18 W can illuminate samples from above on a plate with 4 x 5 magnetic stirring spots.

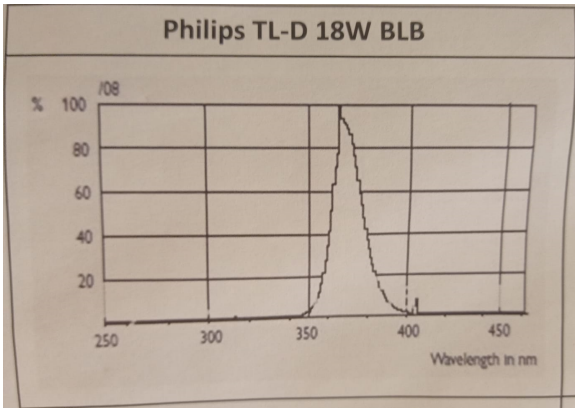

Figure 11: Spectrum of lamps that were used for both dye degradation and photodeposition.

4 Results

In this section the results of different ways of gold cocatalyst deposition onto $SrTiO_3$ particles are described. At the end of this section the dye degradation efficiency of the prepared materials ($SrTiO_3$ particles with different conditions for cocatalyst deposition) are presented and discussed.
Firstly, however, the surface charge/potential values as function of pH and isoelectric points of the entire gold and $SrTiO_3$ particles are measured. For this the Zetasizer nano ZS is used as described in section 3. For familiarization with the instrument and method, first an experiment with a well-known system, namely silica nanoparticles was done. As can be seen in figure 30 the isoelectric point of 22 nm silica particles obtained from these measurements was found at a pH of approximately 2.3. This is in good agreement with work of Aimable et al.(2020), where the point of zero charge (PZC), or isoelectric point, of the same system (same size and provider, namely LUDOX AS-40) was also found at a pH of roughly 2.3. [75] This can be seen in the appendix in figure 30.
The details of the measurement procedure of the zeta potential for all particles in this section can be found in section 3. The isoelectric point of the $SrTiO_3$ particles was quantified and the results of this experiment are shown in figure 13. Herein obtained results (blue circles) qualitatively agree with what is shown in work by Su et al. (2021) (red triangles), although here it is found that the isoelectric point is around pH of 4 as compared to the isoelectric point found at pH of 3.5 found by Su et al.(2021). [47] Also the absolute values of the zeta potential are different especially at a pH lower than 6. This small discrepancy could be explained by slightly different $SrTiO_3$ particles, which were synthesized using a slightly different protocol. Resulting particles have a different size, facet {110} to {100} ratio, and possibly different surface defect density that will affect the whole particle's isoelectric point as described in Su et al.(2021). [47] It should be pointed out that quantifying the absolute values of the zeta potential for this complex/heterogeneous (faceted particle and polydisperse as well as impurities such as TiO_2) system is very challenging.
Using atomic force microscopy (AFM), Su et al. (2021) showed that individual facets of $SrTiO_3$ nanoparticles have different surface charge characteristics and isoelectric points. It can be seen that even if the zeta potential measurement show 0 mV, the facets can still be charged. This becomes clear from the difference in surface charge as measured by AFM compared to the measurement by electrokinetics.
The zeta potential changes as function of pH, likely due to the oxygen atoms at the surface that get protonated by the H^+ ions and the concentration of the H^+ ions decreases as the pH increases. This leads to higher surface charge at lower pH, because more of the surface is protonated by H^+ ions. [76]
In figure 12, it can be observed that the {110} facet has an IEP at approximately pH 4, while the {100} facet has an IEP at approximately pH 6. This indicates that there is a pH window from around 4 to 6, in which the {100} and {110} facets carry opposite charge,

namely the {100} facet is positively charged, while the {110} facet is negatively charged. At a pH between 4 and 6 negatively charged silica particles were selectively adsorbed only on the {100} facet. [47] This phenomenon is exploited here as well to selectively deposit 15 nm gold nanoparticles instead of silica.
The zeta potential as function of pH of 15 nm gold nanoparticles is shown in figure 14. The figure displays that in citrate buffer the particles carry a negative charge for a pH between 2 and 10. This result is in agreement with work of Sun et al.(2009), who also find negative charge for every pH above roughly pH 1, which is attributed to the citrate groups at the surface. [77]

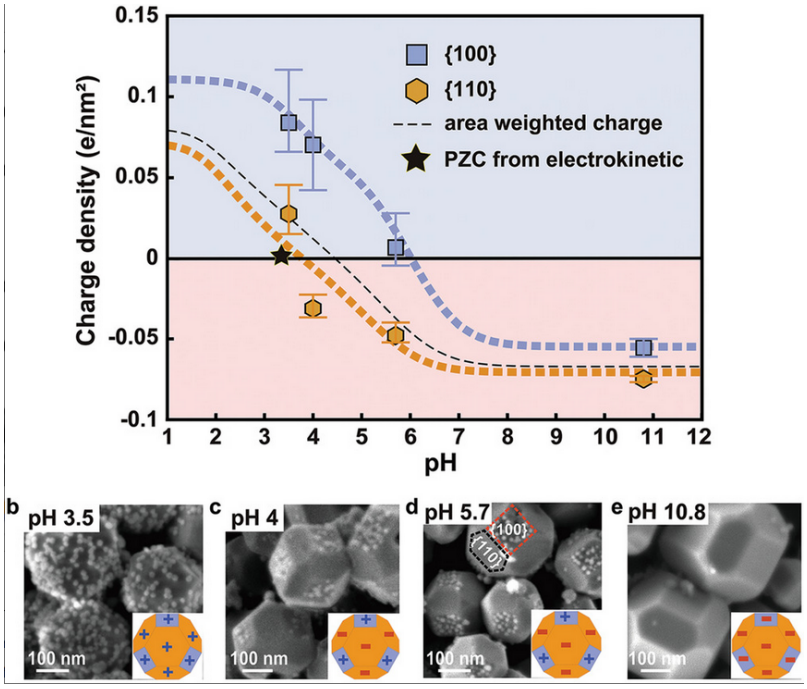

Figure 12: Plot AFM measurements of surface charge of the {100} and {110} facets of $SrTiO_3$ particles as function of pH. In the bottom pictures, silica deposition on $SrTiO_3$ facets is shown with negatively charged silica particles. Taken from Su et al. (2021) [47].

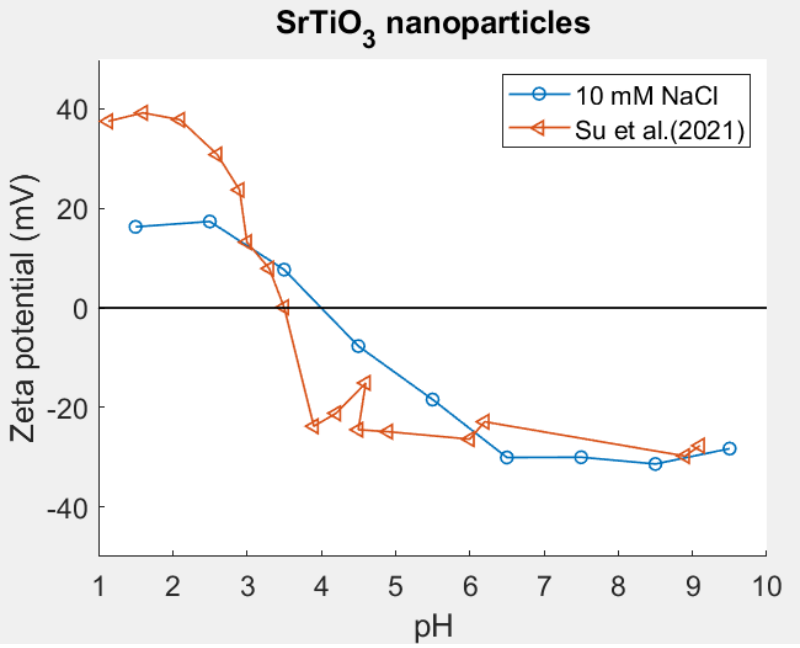

Figure 13: Plot of zeta potential as function of pH for $SrTiO_3$ and compared to measurements done by Su et al. (2021) [47].

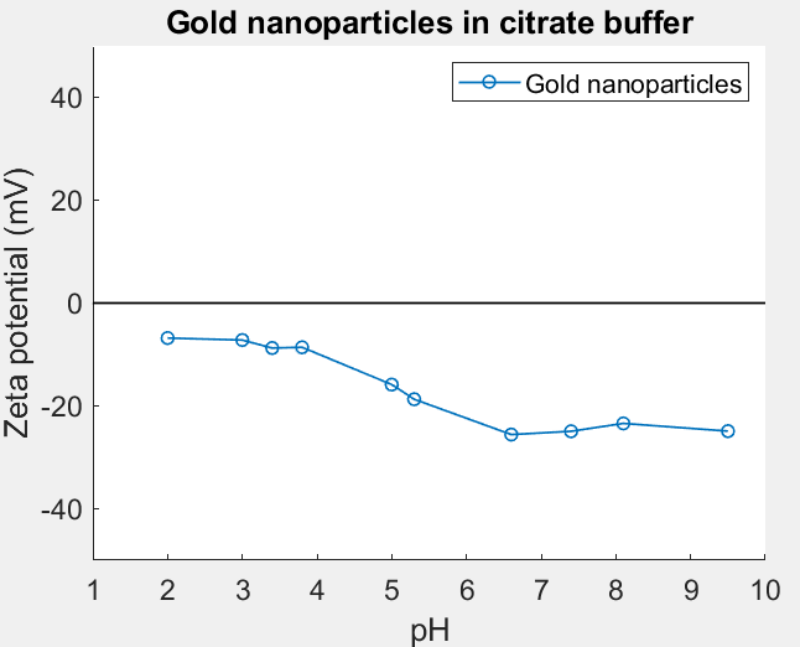

Figure 14: Plot of zeta potential as function of pH for gold nanoparticles in citrate buffer.

4.1 Colloidal deposition of gold

The result of deposition of 15 nm gold nanoparticles on $SrTiO_3$ under 1 mM NaCl fluid compositions are shown in figure15. The sample was characterised in two different SEM imaging modes, namely ESB and InLens modes.More explanation on this can be found in section 3

The purpose of this procedure is to distinguish between gold nanoparticles and TiO_2 residual particles that have similar shape and size. It is possible to use different percentages of ESB and Inlens mode in one picture, which results in pictures where different aspects are highlighted (i.e. the gold nanoparticles appear brighter in images). Due to gold's higher atomic number, with higher ESB imaging mode the gold nanoparticles appear brighter (contrast) compared to TiO_2 particles. In a higher InLens mode, the individual facets of the $SrTiO_3$ particles are more easily identified. Varying levels of ESB and inlens mode are used in these pictures to highlight the gold nanoparticles or the $SrTiO_3$ facets more. An attempt is made to strike a good balance between the two, so that it is clear what is being shown.

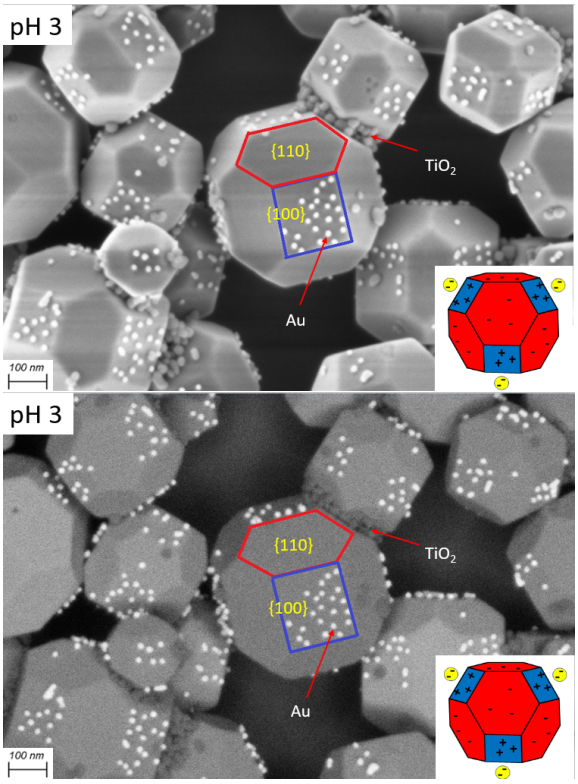

Figure 15: SEM pictures of $SrTiO_3$ with gold colloidal nanoparticles deposited at pH 3, 1 mM NaCl, 1.3 mg gold/2 mg $SrTiO_3$.

The two pictures in figure 15 show the resulting particles after colloidal particle deposition was done using 1.3 mg of gold nanoparticles of 15 nm size with 2 mg of $SrTiO_3$ particles at pH 3 in 1 mM NaCl solution. These pictures are taken at the same location, but with different modes. The top picture is taken in high percentage of InLens mode, while the bottom pciture is taken with a high percentage of ESB mode.
The ESB mode shows that the brighter particles have a higher atomic number than the darker ones. These brighter particles are attributed to be gold nanoparticles, while the darker particles, which are also observed when looking at bare $SrTiO_3$ particles as in figure 16, are attributed to be TiO_2, which was likely left over from the $SrTiO_3$ synthesis process.
Here the square blue-outlined facet is the {100} facet and the hexagonal red-outlined facet is the {110} facet. Importantly these images show that the {100} facets of $SrTiO_3$ are decorated with 15 nm particles that we assign to gold. This suggests that at pH 3 and 1 mM NaCl the negatively charged colloidal gold nanoparticles were attracted to the positively charged {100} facet, while there is electrostatic repulsion between the negative gold nanoparticles and the negatively charged {110} facet. Hence the earlier established proto-

col for facet-selective silica deposition onto $SrTiO_3$ particles by Su et al.(2021) can be used for gold nanoparticles as well! [47]

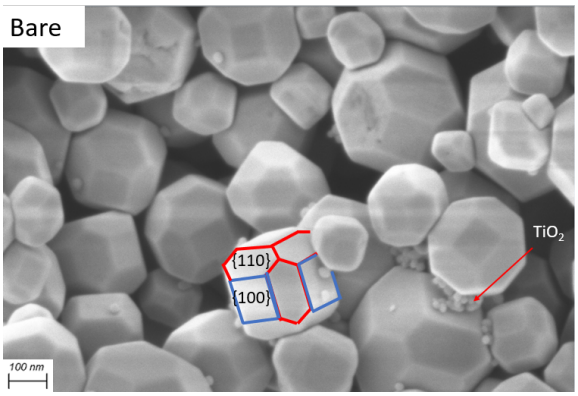

Figure 16: SEM pictures of bare $SrTiO_3$. Some residual TiO_2 can be observed, which is likely leftover from the synthesis process.

The gold nanoparticle deposition performed at different pH of the solution with 10 mM NaCl and 1.3 mg gold / 2 mg $SrTiO_3$ is shown in figure 17. At different pH, as expected, the gold nanoparticle deposition takes place at different facets. As the gold nanoparticle's potential/charge is (virtually) independent of pH, this is the result of changes in the surface charge of individual facets of $SrTiO_3$ particles as shown from AFM measurements by Su et al.(2021). [47] The illustrations in the corner of the image show the proposed surface charge of the facets of the $SrTiO_3$ particle. As expected at pH 2.5 both facets are positively charged, which attract the negatively charged gold particles. In the pH window of 3 to 3.5, facet selective deposition onto the {100} facet can be observed, which is likely caused by the difference in surface charge as outlined above. Finally at pH 5 or higher (virtually) no gold deposition is observed onto the $SrTiO_3$, which is likely due to the negative charge on both facets. These findings overall fit with the pH dependent silica deposition reported by Su et al.(2021), yet it should be pointed out that the pH window over which the facet selective particle deposition takes place is more narrow and is shifted towards a lower pH. [47] This can again be attributed to the slightly different $SrTiO_3$ particles.

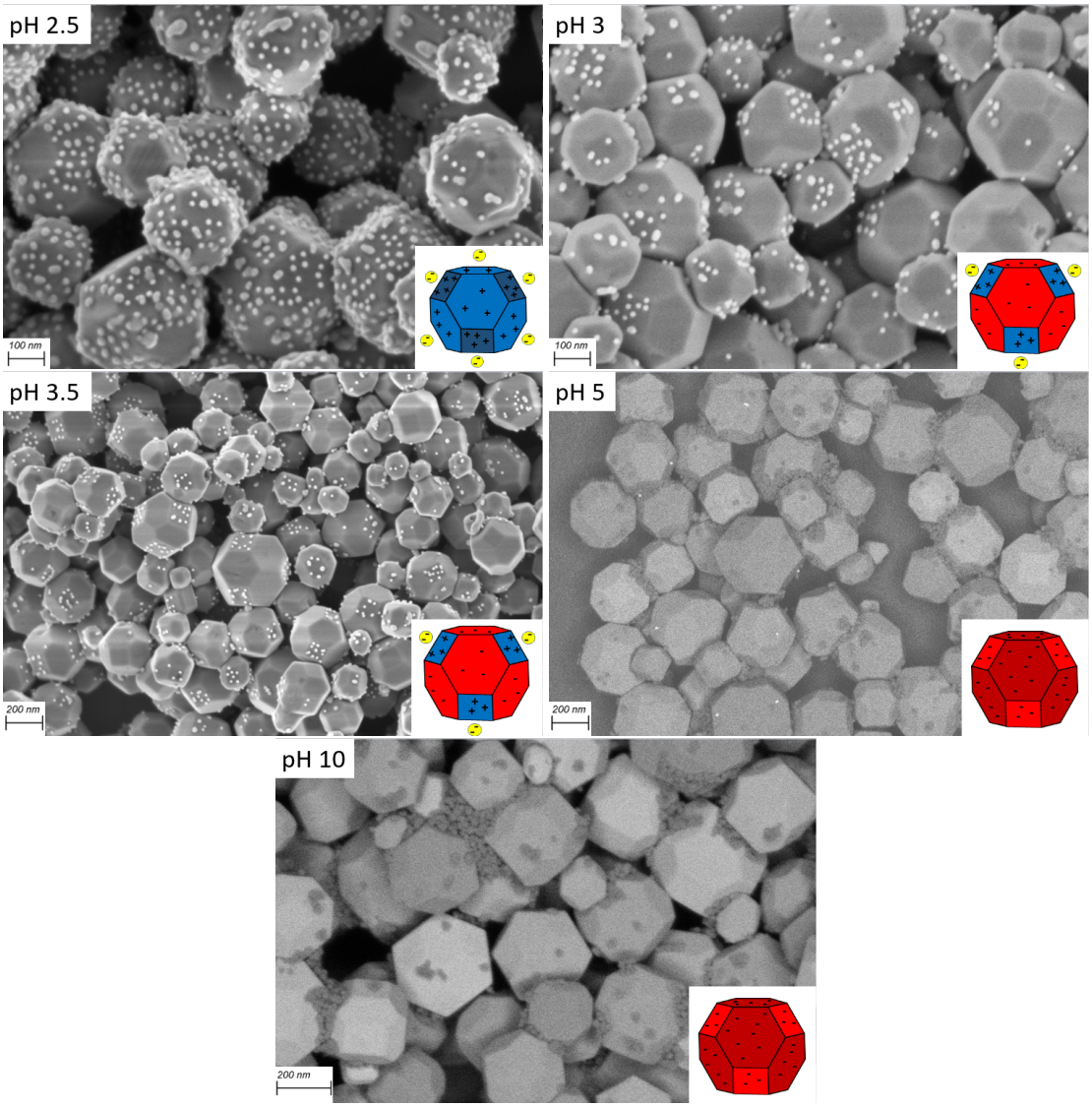

Figure 17: SEM pictures of $SrTiO_3$ with gold colloidal nanoparticles deposited at: from top left to bottom; pH 2.5, 3, 3.5, 5, 10. Done at 10 mM NaCl, 1.3 mg gold/2 mg $SrTiO_3$.

From the experiments above, we learned that, between pH 3 to pH 3.5, facet selective deposition of colloidal gold nanoparticles onto the {100} facet of $SrTiO_3$ is possible. This is likely due to the difference in surface charge of the $SrTiO_3$ nanoparticle facets causing electrical attraction and repulsion of the gold nanoparticles at the {100} and {110} facets respectively.
To test how robust the deposition protocol is and how reproducible the facet selective de-

position of the gold nanoparticles is, more experiments are done using different batches of the particles, with the same protocol: pH 3, 1 mM NaCl, 1.3 mg gold per 2 mg of $SrTiO_3$. The results of these tests can be seen in figure 18.
Here it seems that some batches such as the top two pictures show quite nice facet selectivity, where the vast majority of the gold particles deposit onto the square {100} facet. The rest of the pictures are less clear in their facet selectivity, although generally a preference for the {100} facet can still be distinguished. There is also some variability in terms of gold nanoparticle coverage of the facet. The difference in this behaviour is still unclear. A possible explanation for this is that the facet surface charge of individual particles could depend on the $SrTiO_3$ particle size and defect distribution. [78] The presence of small contaminants from plastic pipettes or glass bottles or from other sources could affect the deposition process. Another explanation could be that there is some contamination caused by any of the instruments that are used in the deposition process and that this could affect surface charge or cause steric hindrance or instability. Note that these are speculations and more research would need to be done to test what is the origin of this irreproducibility of the facet selective gold nanoparticle deposition onto $SrTiO_3$.

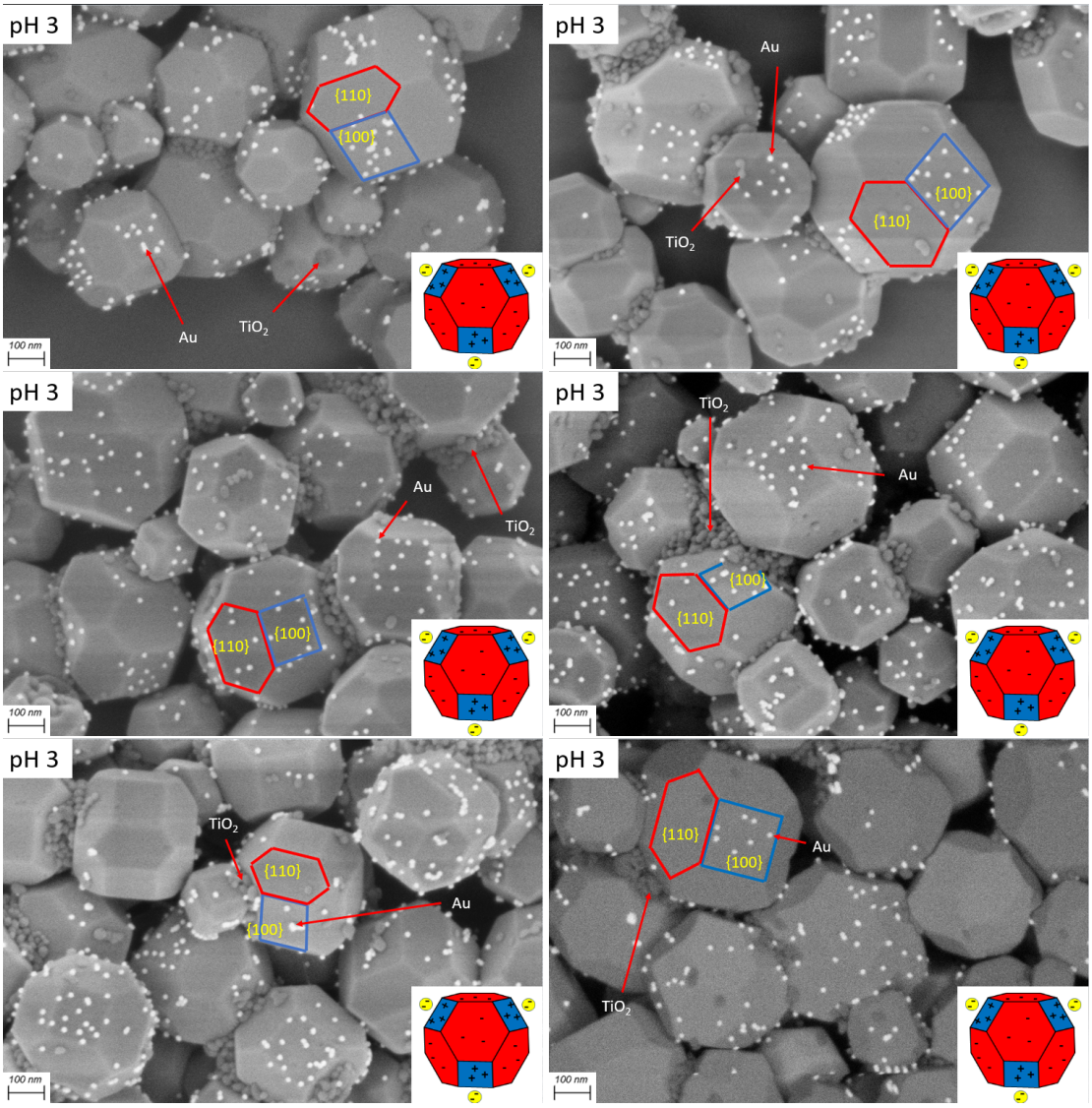

Figure 18: SEM pictures of 6 different batches of $SrTiO_3$ with gold colloidal nanoparticles deposited at pH 3, 1 mM NaCl, 1.3 mg gold/2 mg $SrTiO_3$, produced at different times.

Additionally gold deposition was done at a fixed pH of 3 and fixed gold concentration, but variable NaCl concentration, which can be seen in figure 19. With increasing salt concentration the Debye length reduces, because the ions screen more of the charge of the particle and thus decrease the size of the electric double layer. This could reduce the distance between adsorbed gold nanoparticles, because the electrical repulsion of a gold particle propragates less far. [68]

Debye length was calculated from the following equation 13 for a symmetric monovalent electrolyte and shown in the sketch in the corner of the pictures in figure 19. Here λ_D is the debye length, ε_r and ε_0 are the dielectric constant and the premittivity of free space respectively. R is the gas constant, T is the temperature. Finally F is the faraday constant and C_0 is the electrolyte concentration. [79]

$$\lambda_D = \sqrt{\frac{\varepsilon_r \varepsilon_0 RT}{2 \cdot 10^3 F^2 C_0}} \tag{13}$$

At a salt concentration of 0.5, 1 and 10 mM NaCl the gold nanoparticles are selectively adsorbing only on the {100} facet of $SrTiO_3$.

To assess the average distance between the gold nanoparticles, a Matlab script was developed and used, which can be found in the appendix. The routine finds the center of the gold particles, through thresholding and a function 'regionprops'. Then the distance from each gold particle to its nearest neighbour was calculated and an average for the facet was given. This crude analysis of the data reveals that at 1 mM NaCl the average center-to-center separation distance between particles is roughly 28.95 nm. At 10 mM NaCl this distance is roughly 20.4 nm. So it seems that there is indeed a difference in the gold inter-particle separation and hence the coverage of the facet depending on the salt concentration, namely a higher salt concentration gives rise to a smaller distance between gold nanoparticles. Note that the analysis was done for 4 different facets of each batch.
At 300 mM NaCl, the SEM image shows that the facet-selectivity is gone or reversed. At this salt concentration the Debye length is roughly 0.56 nm, hence the interparticle distance is expected to reduce further, yet this is not observed in our experiments. By increasing the salt concentration, the debye length reduces, but also the surface charge of gold and $SrTiO_3$ particles is effectively screened (electric double layer strength reduced). Hence the short range VanderWaals and the hydration forces would dominate over the electric double layer force. Through manual counting a ratio of gold particles on the {110} to {100} facet of roughly 2:1 is found. Meaning that there are more gold particles deposited onto the {110} facet. A coincidence or not the {110} facet has the weaker hydration structure of the two as measured by Su et al. (2021). [47] In work of Dong et al. (2014) it is reported that the $SrTiO_3$ facet's hydration structure controls the protein adsorption. [69] Yet here again, more experiments and more elaborate analysis are needed for a conclusive statement.

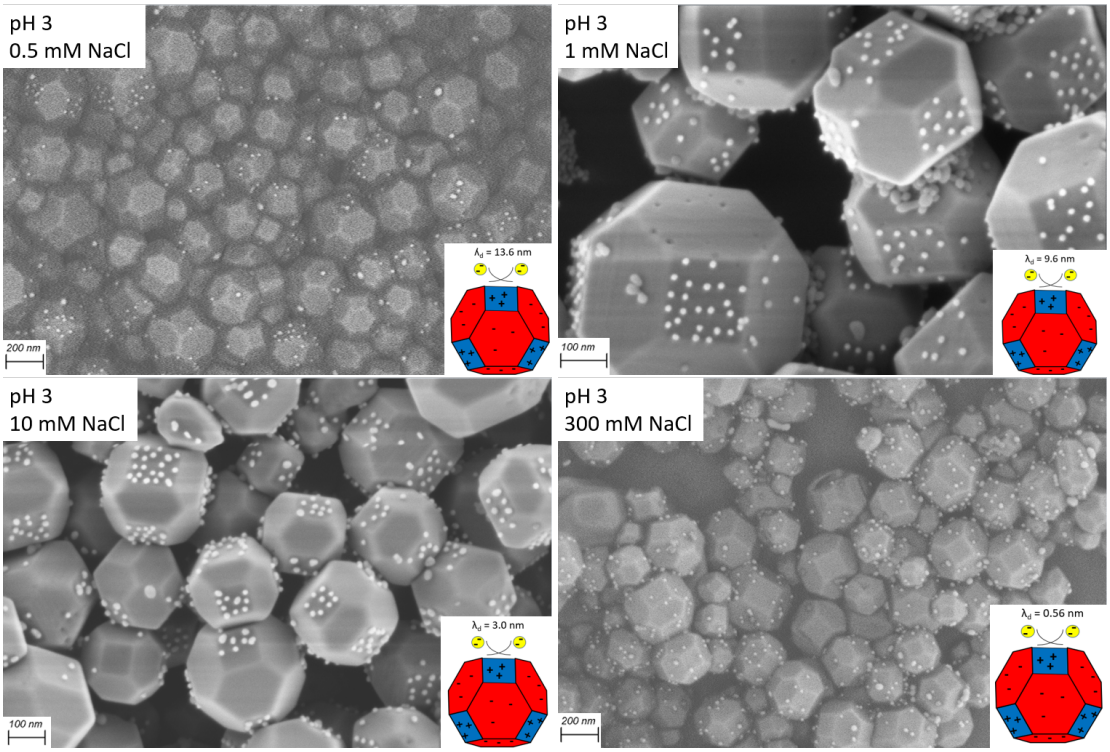

Figure 19: SEM pictures of $SrTiO_3$ with gold colloidal nanoparticles deposited at: from top left to bottom right; 0.5, 1, 10, 300 mM NaCl, pH 3, 1.3 mg gold/2 mg $SrTiO_3$.

Gold deposition on $SrTiO_3$ was also done at three different gold concentrations. Specifically gold concentrations of roughly 0.44 mg, 1.3 mg and 2.6 mg per 2 mg of $SrTiO_3$ at pH 3 and 1 mM NaCl, which is shown in figure 20.

The results of these experiments are not fully conclusive. At all 3 different gold concentrations, there is no significant difference in the amount of deposited gold nanoparticles. Also, at lowest gold concentration 0.44 mg, the facet selectivity is unclear, while for the higher gold nanoparticle concentrations the facet selectivity is preserved and takes place on the {100} facet. This could be a result of variability between experiments, as described in figure 18. Or, a threshold amount of gold is required for good facet-selectivity. What is clear that the selectivity and amount of adsorbed gold is not limited by the bulk concentration of gold nanoparticles. Even at a lower concentration there is more than enough gold particles in the bulk solution as can be seen from the amount of gold on the $SrTiO_3$ particles.

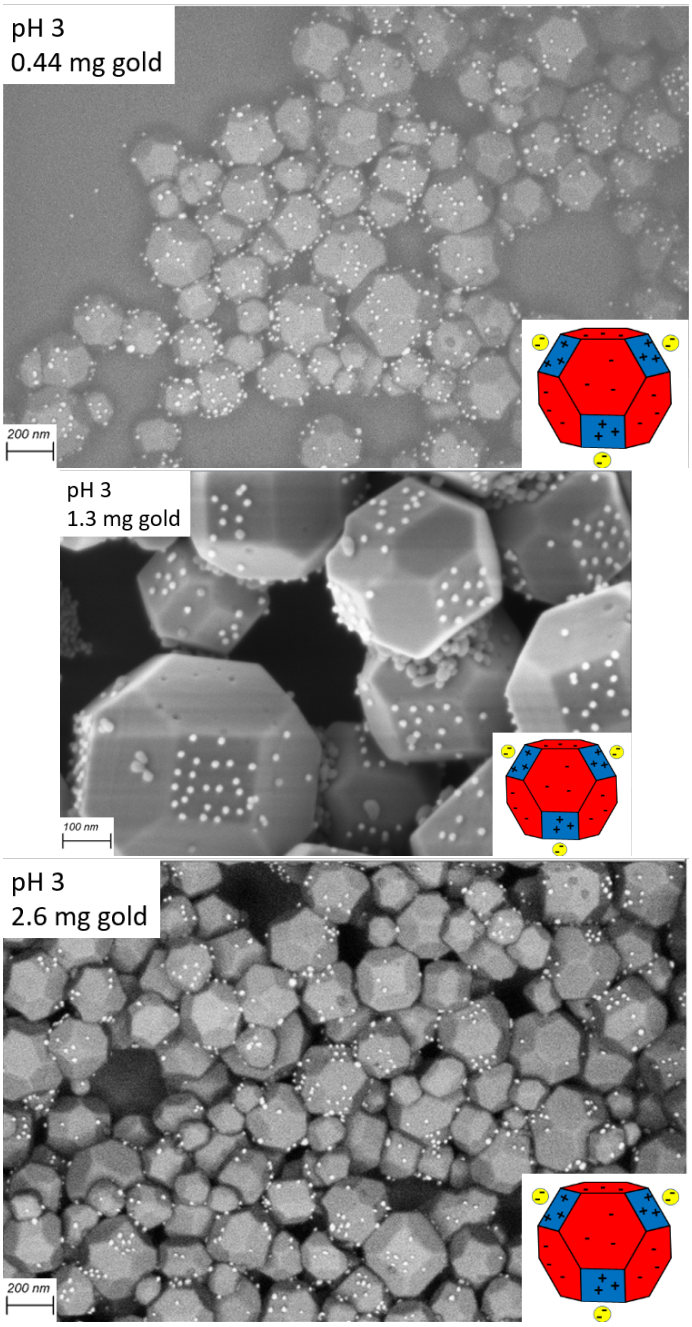

Figure 20: SEM pictures of $SrTiO_3$ with gold colloidal nanoparticles deposited at: from top to bottom; 0.44, 1.3, 2.6 mg gold/2 mg $SrTiO_3$, pH 3, 1mM NaCl.

For a good transfer of photogenerated charges (electrons and holes) from the semiconductor to the cocatalyst-electrolyte interface, therefore there should be a good electrical connection between the gold nanoparticles and $SrTiO_3$ semiconductor nanoparticles. Hence, in an attempt to achieve this, (i.e. improvement of the electronic contact), after cocatalyst deposition we burn away any small organic molecules that were used to stabilize the gold nanoparticles, by thermal annealing. This is done at 450°C for 1 hour. This temperature is chosen because citric acid, which is used to stabilize the gold nanoparticles, decomposes above about 180°C, while the melting points of gold and $SrTiO_3$ are 1064°C and 2080°C respectively. [80] [81] [82] This allows for the decomposition of citric acid, while maintaining the integrity of the $SrTiO_3$ and the gold. An additional benefit might be the improvement of electronic contact between the $SrTiO_3$ and gold, due to small changes at their interfaces. [83] Additionally Liu et al. (2014) does calcination of Au and Ag on $SrTiO_3$ at 400 ° C for 4 hours after photodeposition, which seems to provide good results. [84] The figure 21 shows that after the thermal annealing procedure, the sample did not change. The integrity of gold nanoparticles and their distribution and as well of $SrTiO_3$ particles is (basically) unaffected.

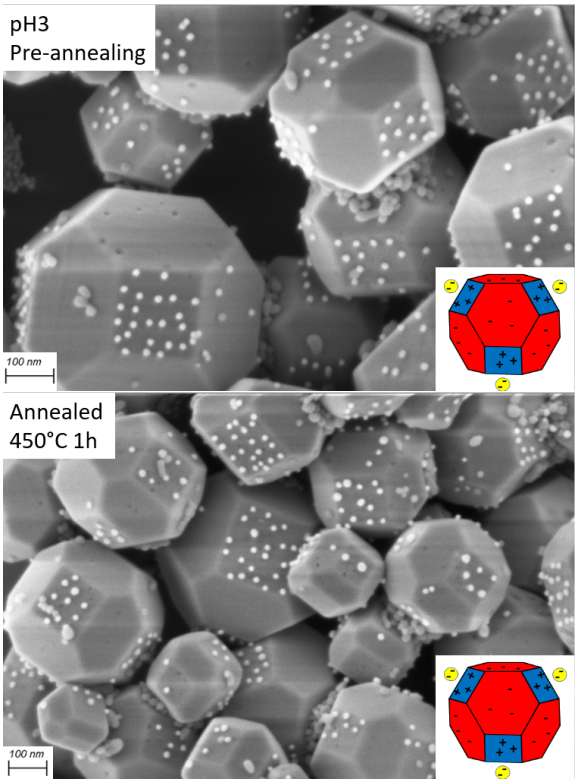

Figure 21: SEM pictures of $SrTiO_3$ with gold colloidal nanoparticles deposited at pH 3, 1 mM NaCl, 1.3 mg gold/2 mg $SrTiO_3$. First picture is made after deposition, while second picture is the same sample after annealing in air at 450 °C for 1 hour.

An important aspect is the stability of the gold cocatalyst nanoparticles on the $SrTiO_3$ after the assembly and eventually during the photocatalytic reaction. To test this gold nanoparticle stability, the following was done: First the gold particle deposition procedure was done onto $SrTiO_3$ at pH 3, 10 mM NaCl, 1.3 mg/ 2 mg of gold/$SrTiO_3$. After this the sample was cleaned, dried and characterized by SEM as described in section 3. The result of this characterisation is shown in figure 22. Additionally half of the sample was redispersed in DI water and stored at room temperature for 1 week. The SEM image show that storing the sample in a solution different than at the deposition conditions (opposite charge of the facets), did not drastically affect the assembly stability of the gold nanoparticles. It can still be seen that the gold nanoparticles are selectively deposited onto {100} facet at (roughly) the same amount. Important to note is that the gold particles stay on the $SrTiO_3$ even if the surface charges change.
In my opinion this is an important aspect in the use in real photocatalytic water splitting and scaling up this process. This seems to be an issue for photodeposited cocatalyst nanoparticles as shown in figure 4 and extensively discussed in work of Mei et al.

(2018). [41] The photodeposited cocatalysts are prone to relocation and rearrangement, dissolution, particle sintering and Ostwald ripening. The result of this is a drastic reduction in photocatalytic activity over time.

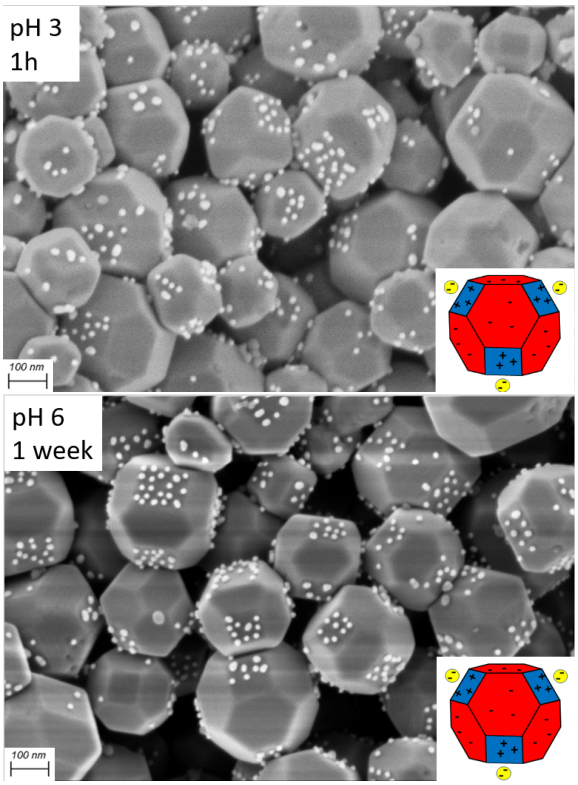

Figure 22: SEM pictures of the same $SrTiO_3$ with gold colloidal nanoparticles deposited at pH 3. Top picture is dried immediately. Bottom picture shows gold-decorated $SrTiO_3$ particles that have been in DI water for at least a week.

What can be learned from this subsection is that facet selective deposition of gold nanoparticles on the {100} facet of $SrTiO_3$ is possible under the right circumstances, where a pH of around 3 seems to be most important. Additionally it seems that using different salt concentrations could provide control over the coverage of the gold nanoparticles on the $SrTiO_3$. Furthermore the gold nanoparticles on the $SrTiO_3$ even without annealing seems very stable for at least a week in suspension. Annealing at a temperature of 450 °C for 1 hour showed minimal to no change in terms of gold nanoparticle coagulation or loss of nanoparticles. Additionally gold nanoparticle concentration was explored.

4.2 Photodeposition

Photodeposition was done as well, with different conditions (pH, illumination time, precursor ion concentration, methanol use), which can be seen in figures 23 to 25. In general photodeposition process follows the reaction described by equations 14,15, where M stands for metal and MO stands for metal-oxide, n is an integer and e and h are electrons and holes respectively. [39]:

$$M^{n+}(aq) + ne^- \rightarrow M(s) \tag{14}$$

$$M^{n+}(aq) + nh^+ + nH_2O \rightarrow MO_n(s) + 2nH^+ \tag{15}$$

In these experiments gold is being deposited so only equation 14 is really relevant, because it is a metal. So specifically the equation is equation 16

$$Au^{3+}(aq) + 3e^- \rightarrow Au(s) \tag{16}$$

Optimum amounts of $HAuCl_4$ used for photodeposition were chosen based on a study by Mu et al. (2016), who report that $SrTiO_3$ with 0.1 wt% of photodeposited gold performed best in terms of water splitting efficiency. [33] They used a 300 W Xe lamp to illuminate the $SrTiO_3$ suspension with $HAuCl_4$ for 2 hours. In this thesis a different illumination setting was used; the sample was illuminated by 8 UV TL tubes of 18 W each were used in a setup that can be seen in figure 10. Hence the effect of illumination time explored. See 3 for more information about this experimental set up.
In order to make a fair comparison, it would make sense to roughly match the amount of gold that is photodeposited to what is seen on the $SrTiO_3$ by colloidal deposition of gold. To achieve this different conditions were investigated by varying the amount of $HAuCl_4$ and the pH. In the process of absorbing light electrons and holes are formed and, as can be seen in figure 16, only electrons are used and therefore an electron donor could be used to accept the holes in order to improve the reactions. For this the effect of methanol is investigated as well.
For all the following pictures the graphic at the bottom right is adapted from Wenderich et al. (2016) [39].
Firstly to see the difference in gold photodeposition as function of pH is explored at 5 wt%, while illuminated for 4 hours under UV. This is shown in figure 23, where it seems that at lower pH the gold cocatalyst clusters more and form larger particles, while they also deposit less homogenously than at higher pH. While at higher pH, the gold deposits onto more particles and form somewhat smaller particles. This decrease in gold particle size as function of pH is also seen on TiO_2 in a study by Iliev et al. (2007). [85].
Additionally it looks like the gold generally deposits on the square $\{100\}$ facet. This is expected because the electrons accumulate at the $\{100\}$ facet, where then the photodeposition reaction happens for the metal cocatalyst. [29]

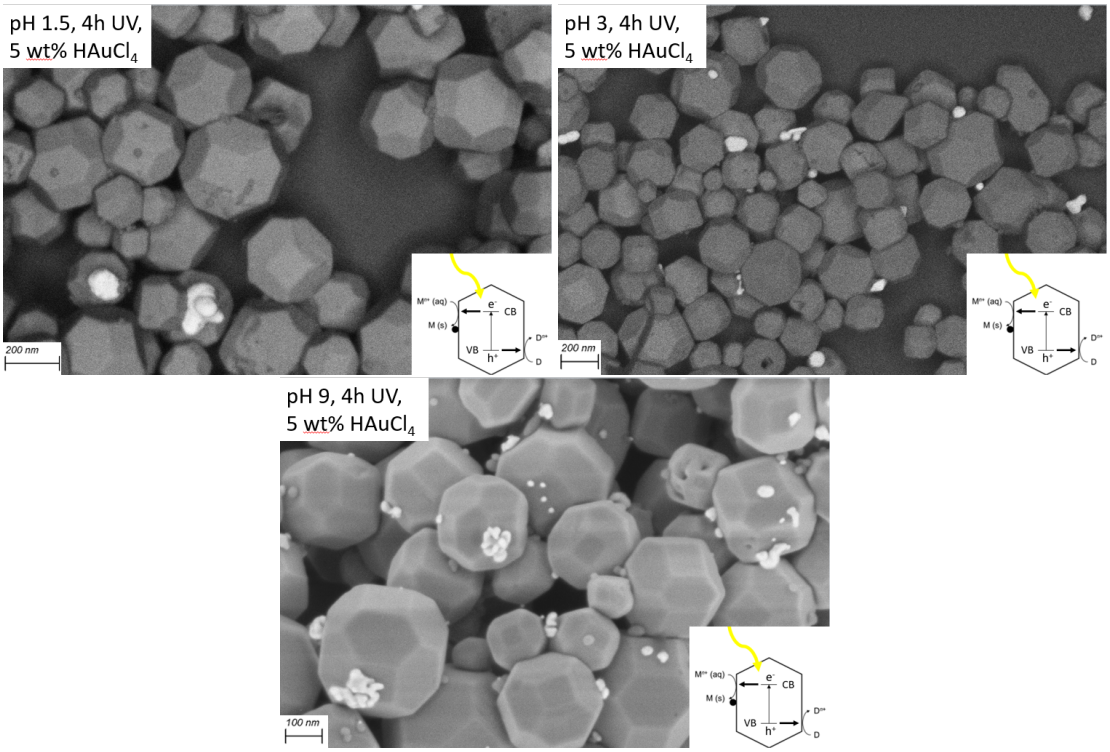

Figure 23: SEM pictures of $SrTiO_3$ with photodeposited gold, illuminated under UV for 4 hours. From top left to bottom: pH 1.5, 3, 9, using 5 wt% $HAuCl_4$.

Using methanol as an electron donor as well as illumination time is investigated in the following figures, 24, 26, 25. 14% methanol was added during the photodeposition in order to improve the photodeposition reaction, based on work by Guo et al. (2018). [86] It seems that the difference when using methanol during photodeposition is clearest in figure 24, where it can be seen that the gold particles become smaller and more scattered over the $SrTiO_3$ particle. The reason for this is unclear, although a possible explanation could be that due to the presence of an electron donor, more photodeposition reactions take place at the surface of the $SrTiO_3$ instead of some kind of precipitation onto the gold surface. This could cause the gold to deposit at more locations instead of growing from an initially deposited gold particle.

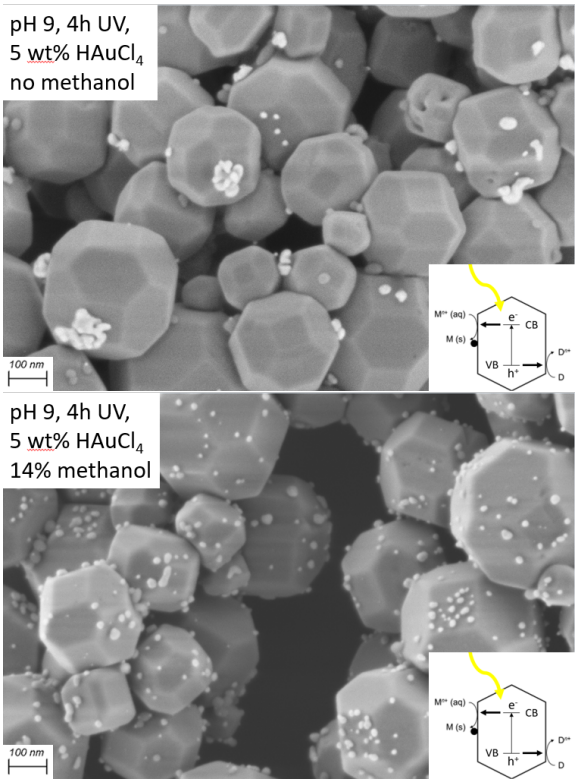

Figure 24: SEM pictures of $SrTiO_3$ with photodeposited gold, illuminated under UV light for 4 hours, top picture: pH 9, 5 wt% $HAuCl_4$, no methanol. Bottom picture: pH 9, 5 wt% $HAuCl_4$, 14% methanol.

In figures 26 and 25 the difference in illumination time and methanol use is shown for a loading of 0.1 wt% of gold on $SrTiO_3$. Figure 25 shows pictures of photodeposition of gold onto $SrTiO_3$ without methanol and with 14% methanol at an illumination time of 4 hours, while figure 26 shows the same but at an illumination time of 2 hours.
The difference in deposition of the gold due to methanol is not very clear due to the small total amount of gold that is deposited. Additionally there does not seem to be a large difference between a illumination time of 2 to 4 hours. This could mean that at 2 hours all of the $HAuCl_4$ has deposited onto the $SrTiO_3$, however this is not clear due to the small amount of gold that is observed, which makes it difficult to make any meaningful comparison between the conditions.

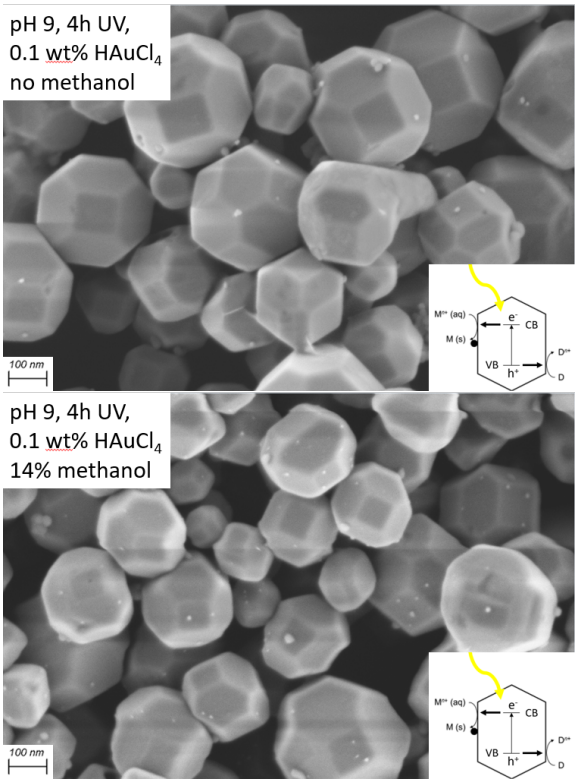

Figure 25: SEM pictures of $SrTiO_3$ with photodeposited gold, illuminated under UV light for 4 hours, top picture: pH 7, 0.1 wt% $HAuCl_4$, no methanol. Bottom picture: pH 7, 0.1 wt% $HAuCl_4$, 14% methanol.

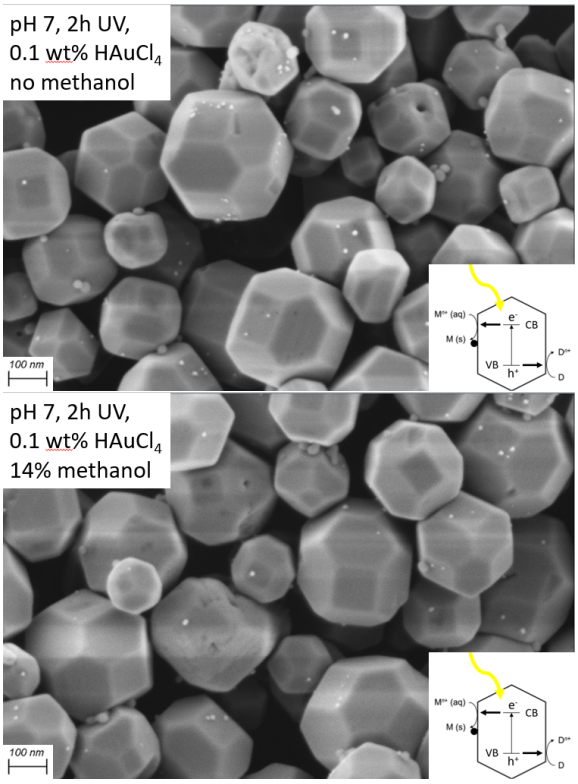

Figure 26: SEM pictures of $SrTiO_3$ with photodeposited gold, illuminated under UV light for 2 hours, top picture: pH 8.8, 0.1 wt% $HAuCl_4$, no methanol. Bottom picture: pH 8.8, 0.1 wt% $HAuCl_4$, 14% methanol.

What can be learned from this subsection is that, as expected, the gold cocatalyst particles are photodeposited selectively on the $\{100\}$ facet of the $SrTiO_3$. A higher amount of gold precursor ions ($HAuCl_4$) results in a higher amount of gold that is photodeposited, although less homogenously. Also the pH of the solution affects the size and distribution of the photodeposited gold, as can be seen in figure 23. The use of a hole scavenger, namely methanol, seemed to have an effect of reducing the size of the deposited gold particles especially for higher amount of gold, as can be seen in figure 24. The illumination time of 2 to 4 hours seems to not drastically affect the photodeposition. When comparing figures 15 and figure 24, one should note that the distribution of the gold cocatalyst nanoparticles in terms of size, arrangement and distribution on the $\{100\}$ facet of the $SrTiO_3$ particles is better using colloidal deposition as compared to photodeposited gold.

4.3 Photocatalytic activity

In the next section we will compare these samples, namely $SrTiO_3$ with gold colloidal nanoparticles and $SrTiO_3$ with photodeposited gold cocatalyst in terms of their photocatalytic performance, assessed by dye degradation of methylene blue. The procedure for this dye degradation can be found in section 3. The pH of each solution was roughly 7 and left unadjusted.
SEM pictures of the batch of $SrTiO_3$ particles that were used for the dye degradation can be seen in figure 27. The different loadings were chosen based on literature by Mu et al. (2016). [33] They found that 0.1 wt% of gold on $SrTiO_3$ performs best in a water splitting context. Furthermore 2 wt% of gold on $SrTiO_3$ was chosen to roughly match the amount of gold that is deposited via gold colloidal deposition. Finally the gold colloidal nanoparticle deposition is also investigated, with two different batches prepared, which can be seen in the bottom pictures. Both are prepared according to the previously established protocol; 1 mM NaCl solution, with 1.3 mg gold per 2 mg $SrTiO_3$ at pH of 3. The bottom left picture will be used as it is, while the bottom right picture will be annealed and then used for dye degradation.
In the bottom left picture a reasonable degree of facet selectivity can be observed, however it is not perfect. And for the bottom right picture the {100} the annealing process seems to have caused the gold nanoparticles to coagulate, which is not desired. This is unexpected, because in a previous experiment, as shown in figure 21 the gold distribution was unaffected by the annealing.

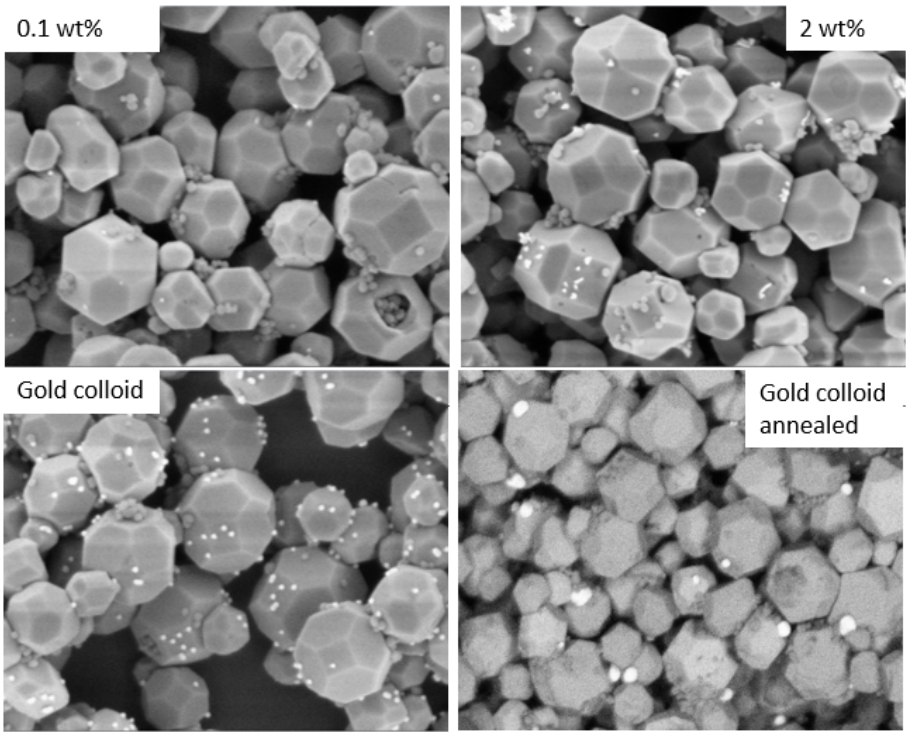

Figure 27: SEM pictures of $SrTiO_3$ with different ways of gold deposition that are used for dye degradation. Top left: Photodeposition with 0.1 wt% of $HAuCl_4$. Top right: Photodeposition with 2 wt% of $HAuCl_4$. Bottom left: gold nanoparticle deposition at pH3, 1 mM NaCl. Bottom right: gold nanoparticle deposition at pH 3, 1 mM NaCl, after annealing.

The results of the dye degradation are shown in figure 28. These points on the graph were produced by taking the peak of the absorbance spectrum from UV-vis spectrometry at 664 nm and dividing this by this peak of the initial dye concentration before any illumination has taken place, which is a common method of visualizing the dye degradation. [44] [45] An example absorbance spectrum of methylene blue can be seen in appendix figure 33. The graph shows the normalised concentration of the methylene blue dye that is left after removing the $SrTiO_3$ particles, as a function of time. A larger decrease in methylene blue concentration indicates that the photocatalyst performs better. [87]
As expected for the control sample (no $SrTiO_3$ particle present in the solution, green crossed line), the methylene blue concentration is stable over the course of 7 hours of illumination. When the solution is illuminated with $SrTiO_3$ particles with gold cocatalyst present, we see that the normalised dye concentration (C/C_0) decreases in time. This indicates that the photocatalyst degrades the dye. The $SrTiO_3$ particles with a loading of 0.1 wt% (blue line with circles) by photodeposition seem to perform the better than the 2 wt% loading, as expected based on work by Mu et al. (2016), who tested the same materials on

hydrogen evolution efficiency. [33]
When comparing $SrTiO_3$ with 2 wt% photodeposited gold (red line with plusses) with $SrTiO_3$ with gold colloidally adsorbed nanoparticles (yellow line with triangles) that visually show a similar amount of gold, the latter shows slightly higher dye degradation efficiency of methylene blue. The annealing of the sample (purple line with triangles) further increases the dye degradation efficiency. Another explanation of this could be that there is less gold particles on the sample.
This time the annealing process seems to affect the sample, because it can be seen that the gold nanoparticles have accumulated into larger clumps as can be seen in figure 29. The origin is unclear, because the temperature of the annealing is far from the melting temperature of gold. This means that there is potential to optimise the annealing process further. Even still it seems that these $SrTiO_3$ particles with annealed gold perform better than their non-annealed counterpart. This is likely because of the improved electrical contact of the colloidally deposited gold particles with the semiconductor. It is clear that the $SrTiO_3$ particles with 0.1 wt% of photodeposited gold performs better in terms of dye degradation than the $SrTiO_3$ with colloidally deposited gold. A reason could be that a lower amount of gold performs better, and that the current loading of gold by colloidal nanoparticle deposition is too high and not optimized here.

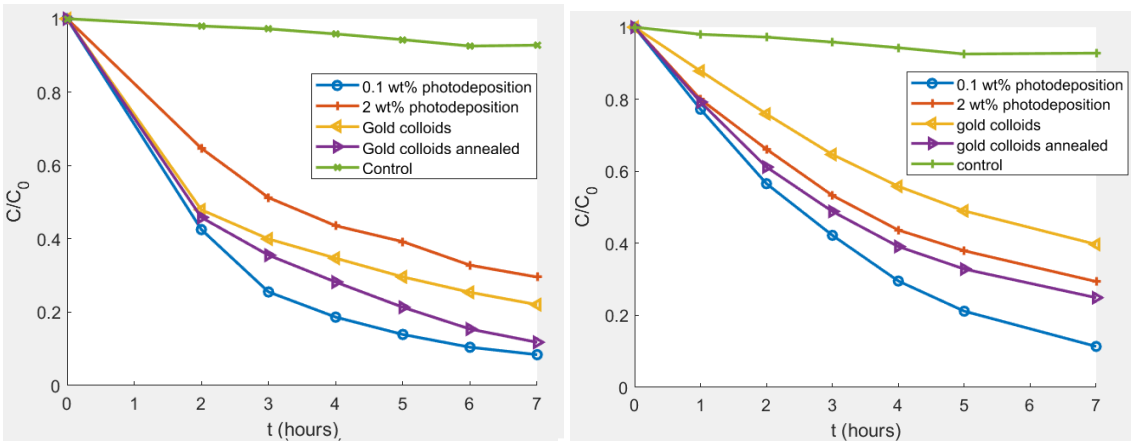

Figure 28: Plot of normalised concentration of Methylene Blue as function of illumination time using $SrTiO_3$ particles for photodegradation. For this the same particles were used as in figure 27 and 29. The left picture shows the first cycle, while the right picture shows a second cycle of dye degradation, after recovering and cleaning the particles.

The gold-decorated $SrTiO_3$ particles were recovered, cleaned and used for a second dye degradation experiment, which is shown in the right plot of figure 28. SEM images of the particles after the dye degradation are shown in figure 29.
The 0.1 wt% photodeposited (blue line with circles) and the colloidally deposited an-

nealed $SrTiO_3$ particles (purple line with triangles) show similar dye degradation efficiency as the first experiment. However the 2 wt% photodeposited particles perform better than in the previous cycle. The SEM analysis of the sample as shown in figure 29 shows that after first cycle of dye degradation a lot of the photodeposited gold particles were detached from the $SrTiO_3$, this expected based on the work of Mei et al(2018). [41] Also as expected a lower amount of photodeposited gold (closer to the optimum of 0.1 wt%) results in a better dye degradation activity observed and explains why it performs better in the second cycle. This also indicates that this method of photodepositing gold is not very stable.
The $SrTiO_3$ with colloidally deposited gold nanoparticles without annealing (yellow line with triangles) also has a reduction in their activity compared to the first cycle. The origin is unclear at the moment, since there is no significant difference between the samples before and after dye degradation, such as detachment of the gold nanoparticles during the recovery process or photocatalytic reaction.

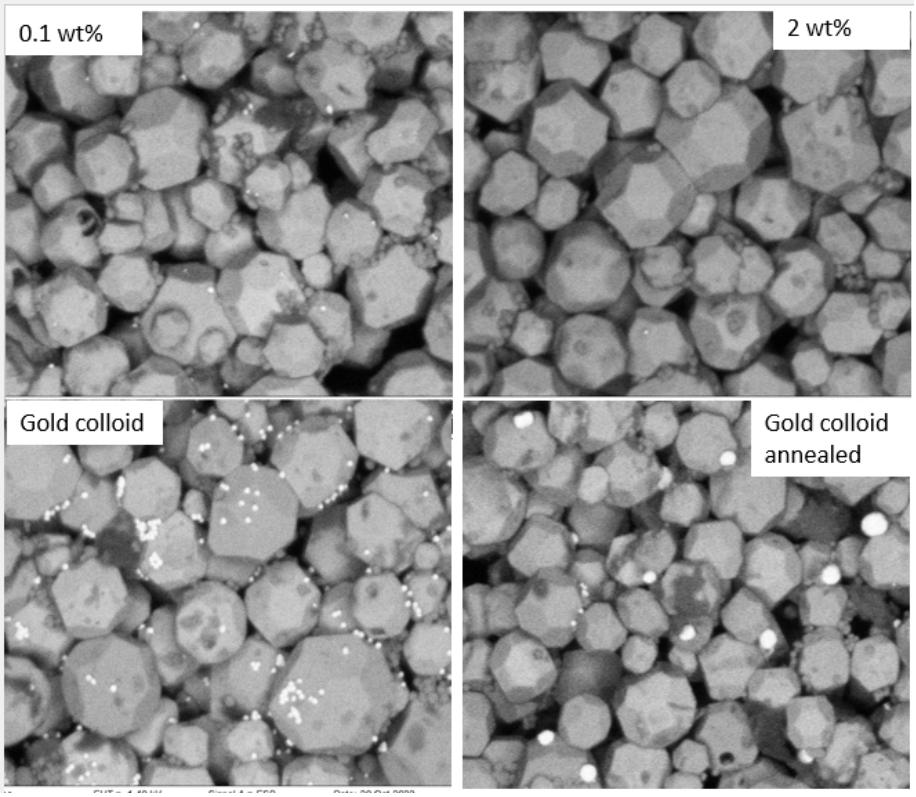

Figure 29: SEM pictures of $SrTiO_3$ with different ways of gold deposition after dye degradation with methylene blue. Top left: Photodeposition with 0.1 wt% of $HAuCl_4$. Top right: Photodeposition with 2 wt% of $HAuCl_4$. Bottom left: gold nanoparticle deposition at pH3, 1 mM NaCl. Bottom right: gold nanoparticle deposition at pH 3, 1 mM NaCl, after annealing.

The dye degradation experiments are not as straightforward as expected and the second repeat experiment of nominally the same dye degradation experiments gives quite different results. All samples seem to perform equally poor and unexpectedly are very close to the bare $SrTiO_3$ without any cocatalyst as can be seen in figure 32 in the appendix. It should be pointed out that the methylene blue dye degradation happens most directly through oxidation reaction, directly via holes or formation of OH radicals. Here via depositing a gold cocatalyst at the $\{100\}$ facet, we optimize for electron transfer. Hence the limiting factor might be the hole transfer, which is not optimized for here.
From these experiments the photocatalytic efficiency is not very conclusive. Assessing the efficiency of the materials presented here, requires more experiments in terms of reproducibility or design (metal-oxide cocatalyst on the other facet, fluid composition, a different dye or hydrogen evolution reaction).

5 Conclusion and recommendations

In conclusion to recap this thesis, several things can be concluded and a few recommendations and additional thoughts will be given.
It can be concluded that gold nanoparticles can be facet selectively adsorbed via DLVO forces onto faceted $SrTiO_3$ particles under the conditions shown in section 4. This is achieved at pH 3, 1 mM and 10 mM NaCl, with negatively charged nanoparticles adsorbed onto the postively charged {100} facet of $SrTiO_3$. At lower pH or extremely high salt concentration the facet selectively is lost. Additionally it is clear that the particles are stable on the $SrTiO_3$ when gold is deposited using pre-formed gold nanoparticles. Furthermore the annealing does not affect the shape and distribution of the particles, although this may require further optimization. Importantly the proposed method of cocatalyst deposition shows better control in terms of size, shape and distribution of gold as compared to photodeposition. The photocatalytic performance of this material and how it compares to samples with photodeposited gold here are inconclusive and require further exploration.
Important to note is that if one can get a better or comparable performance, but a better stability, can be a breakthrough or a big step in the photocatalytic community.

5.1 recommendations

This new method of depositing cocatalysts can lead to many different paths of research. An important factor to more accurately assess the impact of this method of cocatalyst deposition for water splitting is that hydrogen evolution could be done for instance, while a hole scavenger such as methanol or a metal oxide cocatalyst on the {110} facet could be used to increase the reaction.
Additionally the effect of different sizes, shapes and materials as a colloidal particle for this cocatalyst deposition could be investigated in terms of its hydrogen evolution. Postively surface charged particles might also be used to facet selectively target the {110} facet.
Occasionally there are samples with smaller amounts of gold deposited. This could happen during the initial deposition process or potentially they come off during the sonication process.
Another question is; what is happening exactly in the washing procedure? Does it start with a lot of gold on the particles, while some more weakly bound particles come off? or are they already in the final configuration? I think some experiments can be done in that area, because this could potentially explain some differences in the reproducibility.
Additionally a setup could be conceived where a confocal microscope could be used in order to investigate what is happening in the suspension when the gold is added or the pH is adjusted.

Finally a noteworthy observation is that the VanderWaals force between the gold nanoparticles and $SrTiO_3$ seems really strong, because the gold colloidal nanoparticles easily stay on the $SrTiO_3$ even without any annealing.

5.2 What did I learn?

In this subsection I want to outline what I learned in this process of working on a project in a research group for an extended period of time.
Firstly I learned a lot of practical skills, such as how the synthesis works of the faceted $SrTiO_3$ particles and how to do the deposition of gold particles. Additionally I learned how to operate machines I never used before and how they work, such as a Zetasizer, UV-vis spectrometer and photodeposition reactor.
I learned a lot theoretically of how the particles behave and how everything happens on a micro or nanoscale. Another thing I learned is that this is not as easy as it looks and using seemingly the same starting conditions and protocols can yield different results. I also learned how complex these nanoscale processes can be and how no one fully understands this, due to limitations of the means to observe the processes at this scale.
I learned interpersonal scales and how to plan better. I had to learn to set priorities, when different people can tell you to do different things and it can feel like a lot to do in a short period of time. Lastly I learned how kind and welcoming people from other research groups can be when allowing me to use their labs and equipment, while taking the time to teach me how to use the equipment and even helping me think of the specific setup to use for the experiments.

Acknowledgements

I would like to offer many thanks to my supervisors Igor Sîretanu, Frieder Mugele, and Shaoqiang Su. They have been invaluable in helping me understand many parts of the project as well as being a great guidance. Thanks to everyone at the physics of complex fluids (PCF) group as well for being open and welcoming and having a great time during my stay at the group. Additionally Bastian Mei and Marco Altomare from the photocatalytic synthesis (PCS) group provided great insight. The PCS group in general has been especially kind in allowing the use of their equipment, expertise and advice for synthesis and measurements. Thanks to Mark Smithers as well from the MESA+ nanolab, for providing me with very nice SEM pictures. Other thanks go out to the people from the Bioelectronics and Nanobiophysics group with whom we have had nice lectures at 11:00 on Tuesdays. They have been a great help as well in offering their lab for measurements, which has given great insight.

References

[1] CBS. (2021) How much energy is from renewable sources? - the netherlands in numbers 2021 — cbs. [Online]. Available: https://longreads.cbs.nl/the-netherlands-in-numbers-2021/how-much-energy-is-from-renewable-sources/

[2] E. Commission. (2014) 2030 climate energy framework. [Online]. Available: https://ec.europa.eu/clima/eu-action/climate-strategies-targets/2030-climate-energy-framework_en

[3] I. E. Agency, "Review 2021 assessing the effects of economic recoveries on global energy demand and co 2 emissions in 2021 global energy," 2021. [Online]. Available: www.iea.org/t&c/

[4] H. Ritchie, M. Roser, and P. Rosado, "Energy," *Our World in Data*, 11 2020. [Online]. Available: https://ourworldindata.org/energyhttps://ourworldindata.org/renewable-energy

[5] T. M. Gür, "Review of electrical energy storage technologies, materials and systems: challenges and prospects for large-scale grid storage," *Energy Environmental Science*, vol. 11, pp. 2696–2767, 10 2018. [Online]. Available: https://pubs.rsc.org/en/content/articlehtml/2018/ee/c8ee01419ahttps://pubs.rsc.org/en/content/articlelanding/2018/ee/c8ee01419a

[6] Augustine, Bain, Chapman, Denholm, Drury, Hall, DG, Lantz, Margolis, Thresher, Sandor, Bishop, Na, Brown, SR, Cada, GF, Felker, Fernandez, SJ, Goodrich, Ac, Hagerman, Heath, ONeil, Paquette, Tegen, and Young, "Renewable electricity

futures study renewable electricity generation and storage technologies volume 2 of 4," 2012. [Online]. Available: http://www.nrel.gov/analysis/re_futures/.

[7] A. I. Osman, N. Mehta, A. M. Elgarahy, M. Hefny, A. Al-Hinai, A. H. Al-Muhtaseb, and D. W. Rooney, "Hydrogen production, storage, utilisation and environmental impacts: a review," *Environmental Chemistry Letters 2021 20:1*, vol. 20, pp. 153–188, 10 2021. [Online]. Available: https://link.springer.com/article/10.1007/s10311-021-01322-8

[8] D. Parra, L. Valverde, F. J. Pino, and M. K. Patel, "A review on the role, cost and value of hydrogen energy systems for deep decarbonisation," *Renewable and Sustainable Energy Reviews*, vol. 101, pp. 279–294, 3 2019.

[9] U. D. of energy, "State of the states: Fuel cells in america 2017," 2018.

[10] E. Commission, "Committee and the committee of the regions a hydrogen strategy for a climate-neutral europe," 2020. [Online]. Available: https://www.eu2018.at/calendar-events/political-events/BMNT-

[11] IEA, "The future of hydrogen," *IEA*, 2019. [Online]. Available: https://www.iea.org/reports/the-future-of-hydrogen

[12] S. Satyapal. (2017) Hydrogen: A clean, flexible energy carrier — department of energy. [Online]. Available: https://www.energy.gov/eere/articles/hydrogen-clean-flexible-energy-carrier

[13] H. I. Villafán-Vidales, C. A. Arancibia-Bulnes, D. Riveros-Rosas, H. Romero-Paredes, and C. A. Estrada, "An overview of the solar thermochemical processes for hydrogen and syngas production: Reactors, and facilities," *Renewable and Sustainable Energy Reviews*, vol. 75, pp. 894–908, 2017.

[14] C. M. Kalamaras, A. M. Efstathiou, Y. Al-Assaf, and A. Poullikkas, "Conference paper hydrogen production technologies: Current state and future developments," *Conference Papers in Energy*, vol. 2013, 2013. [Online]. Available: http://dx.

[15] A. Sharma and S. K. Arya, "Hydrogen from algal biomass: A review of production process," *Biotechnology Reports*, vol. 15, p. 63, 9 2017. [Online]. Available: /pmc/articles/PMC5491395//pmc/articles/PMC5491395/?report=abstracthttps://www.ncbi.nlm.nih.gov/pmc/articles/PMC5491395/

[16] S. Y. Reece, J. A. Hamel, K. Sung, T. D. Jarvi, A. J. Esswein, J. J. Pijpers, and D. G. Nocera, "Wireless solar water splitting using silicon-based semiconductors and earth-abundant catalysts," *Science*, vol. 334, pp. 645–648, 11 2011. [Online]. Available: https://www.science.org/doi/10.1126/science.1209816

[17] W. energy council, "Innovation insights brief 2019 new hydrogen economy-hope or hype?" 2019.

[18] C. H. Partnership, "Hydrogen roadmap europe a sustainable pathway for the european energy transition," 2019.

[19] G. Kakoulaki, I. Kougias, N. Taylor, F. Dolci, J. Moya, and A. Jäger-Waldau, "Green hydrogen in europe – a regional assessment: Substituting existing production with electrolysis powered by renewables," *Energy Conversion and Management*, vol. 228, p. 113649, 1 2021.

[20] S. S. Kumar and V. Himabindu, "Hydrogen production by pem water electrolysis – a review," *Materials Science for Energy Technologies*, vol. 2, pp. 442–454, 12 2019.

[21] C. Zhang, C. Jia, Y. Cao, Y. Yao, S. Xie, S. Zhang, and H. Lin, "Water-assisted selective hydrodeoxygenation of phenol to benzene over the ru composite catalyst in the biphasic process," *Green Chemistry*, vol. 21, pp. 1668–1679, 4 2019. [Online]. Available: https://pubs.rsc.org/en/content/articlehtml/2019/gc/c8gc04017fhttps://pubs.rsc.org/en/content/articlelanding/2019/gc/c8gc04017f

[22] K. Maeda, M. Higashi, D. Lu, R. Abe, and K. Domen, "Efficient nonsacrificial water splitting through two-step photoexcitation by visible light using a modified oxynitride as a hydrogen evolution photocatalyst," *Journal of the American Chemical Society*, vol. 132, pp. 5858–5868, 4 2010. [Online]. Available: https://pubs.acs.org/doi/full/10.1021/ja1009025

[23] R. Li, F. Zhang, D. Wang, J. Yang, M. Li, J. Zhu, X. Zhou, H. Han, and C. Li, "Spatial separation of photogenerated electrons and holes among {010} and {110} crystal facets of bivo4," *Nature Communications 2013 4:1*, vol. 4, pp. 1–7, 2 2013. [Online]. Available: https://www.nature.com/articles/ncomms2401

[24] C. Acar, C. Zamfirescu, I. Dincer, and G. F. Naterer, "Review of photocatalytic water-splitting methods for sustainable hydrogen production related papers a review on select ed het erogeneous phot ocat alyst s for hydrogen product ion review of photocatalytic water-splitting methods for sustainable hydrogen production," 2016.

[25] S. Chen, T. Takata, and K. Domen, "Particulate photocatalysts for overall water splitting," *Nature Reviews Materials 2017 2:10*, vol. 2, pp. 1–17, 8 2017. [Online]. Available: https://www.nature.com/articles/natrevmats201750

[26] A. Fujishima and K. Honda, "Electrochemical photolysis of water at a semiconductor electrode," *Nature 1972 238:5358*, vol. 238, pp. 37–38, 1972. [Online]. Available: https://www.nature.com/articles/238037a0

[27] L. Yuan, C. Han, M. Q. Yang, and Y. J. Xu, "Photocatalytic water splitting for solar hydrogen generation: fundamentals and recent advancements," *http://dx.doi.org/10.1080/0144235X.2015.1127027*, vol. 35, pp. 1–36, 1 2016. [Online]. Available: https://www.tandfonline.com/doi/abs/10.1080/0144235X.2015.1127027

[28] J. Jia, L. C. Seitz, J. D. Benck, Y. Huo, Y. Chen, J. W. D. Ng, T. Bilir, J. S. Harris, and T. F. Jaramillo, "Solar water splitting by photovoltaic-electrolysis with a solar-to-hydrogen efficiency over 30*Nature Communications 2016 7:1*, vol. 7, pp. 1–6, 10 2016. [Online]. Available: https://www.nature.com/articles/ncomms13237

[29] T. Takata, J. Jiang, Y. Sakata, M. Nakabayashi, N. Shibata, V. Nandal, K. Seki, T. Hisatomi, and K. Domen, "Photocatalytic water splitting with a quantum efficiency of almost unity," *Nature 2020 581:7809*, vol. 581, pp. 411–414, 5 2020. [Online]. Available: https://www.nature.com/articles/s41586-020-2278-9

[30] H. Nishiyama, T. Yamada, M. Nakabayashi, Y. Maehara, M. Yamaguchi, Y. Kuromiya, Y. Nagatsuma, H. Tokudome, S. Akiyama, T. Watanabe, R. Narushima, S. Okunaka, N. Shibata, T. Takata, T. Hisatomi, and K. Domen, "Photocatalytic solar hydrogen production from water on a 100-m2 scale," *Nature 2021 598:7880*, vol. 598, pp. 304–307, 8 2021. [Online]. Available: https://www.nature.com/articles/s41586-021-03907-3

[31] T. Setoyama, T. Takewaki, K. Domen, and T. Tatsumi, "The challenges of solar hydrogen in chemical industry: how to provide, and how to apply?" *Faraday Discussions*, vol. 198, pp. 509–527, 6 2017. [Online]. Available: https://pubs-rsc-org.ezproxy2.utwente.nl/en/content/articlehtml/2017/fd/c6fd00196chttps://pubs-rsc-org.ezproxy2.utwente.nl/en/content/articlelanding/2017/fd/c6fd00196c

[32] J. Yang, D. Wang, H. Han, and C. Li, "Roles of cocatalysts in photocatalysis and photoelectrocatalysis," *Accounts of Chemical Research*, vol. 46, pp. 1900–1909, 8 2013. [Online]. Available: https://pubs.acs.org/doi/full/10.1021/ar300227e

[33] L. Mu, Y. Zhao, A. Li, S. Wang, Z. Wang, J. Yang, Y. Wang, T. Liu, R. Chen, J. Zhu, F. Fan, R. Li, and C. Li, "Enhancing charge separation on high symmetry srtio 3 exposed with anisotropic facets for photocatalytic water splitting," *Energy Environmental Science*, vol. 9, pp. 2463–2469, 7 2016. [Online]. Available: https://pubs.rsc.org/en/content/articlehtml/2016/ee/c6ee00526hhttps://pubs.rsc.org/en/content/articlelanding/2016/ee/c6ee00526h

[34] P. Sabatier, *La catalyse en chimie organique*, 1920.

[35] S. Trasatti, "Work function, electronegativity, and electrochemical behaviour of metals: Iii. electrolytic hydrogen evolution in acid solutions," *Journal of Electroanalytical Chemistry and Interfacial Electrochemistry*, vol. 39, pp. 163–184, 9 1972.

[36] T. Kawawaki, M. Kawachi, D. Yazaki, Y. Akinaga, D. Hirayama, and Y. Negishi, "Development and functionalization of visible-light-driven water-splitting photocatalysts," *Nanomaterials 2022, Vol. 12, Page 344*, vol. 12, p. 344, 1 2022. [Online]. Available: https://www.mdpi.com/2079-4991/12/3/344/htmhttps://www.mdpi.com/2079-4991/12/3/344

[37] Y. Nakibli, Y. Mazal, Y. Dubi, M. Wächtler, and L. Amirav, "Size matters: Cocatalyst size effect on charge transfer and photocatalytic activity," *Nano Letters*, vol. 18, pp. 357–364, 1 2018. [Online]. Available: https://pubs.acs.org/doi/full/10.1021/acs.nanolett.7b04210

[38] S. Cao, H. Li, Y. Li, B. Zhu, and J. Yu, "Dependence of exposed facet of pd on photocatalytic h2-production activity," *ACS Sustainable Chemistry and Engineering*, vol. 6, pp. 6478–6487, 5 2018. [Online]. Available: https://pubs.acs.org/doi/full/10.1021/acssuschemeng.8b00259

[39] K. Wenderich and G. Mul, "Methods, mechanism, and applications of photodeposition in photocatalysis: A review," *Chemical Reviews*, vol. 116, pp. 14 587–14 619, 12 2016. [Online]. Available: https://pubs.acs.org/doi/full/10.1021/acs.chemrev.6b00327

[40] M. Carraro, A. Sartorel, F. M. Toma, F. Puntoriero, F. Scandola, S. Campagna, M. Prato, and M. Bonchio, "Artificial photosynthesis challenges: Water oxidation at nanostructured interfaces," *Topics in Current Chemistry*, vol. 303, pp. 121–150, 2011. [Online]. Available: https://www.researchgate.net/publication/51103211_Artificial_Photosynthesis_Challenges_Water_Oxidation_at_Nanostructured_Interfaces

[41] B. Mei, K. Han, and G. Mul, "Driving surface redox reactions in heterogeneous photocatalysis: The active state of illuminated semiconductor-supported nanoparticles during overall water-splitting," *ACS Catalysis*, vol. 8, pp. 9154–9164, 10 2018. [Online]. Available: https://pubs.acs.org/doi/full/10.1021/acscatal.8b02215

[42] C. K. Tsung, J. N. Kuhn, W. Huang, C. Aliaga, L. I. Hung, G. A. Somorjai, and P. Yang, "Sub-10 nm platinum nanocrystals with size and shape control: Catalytic study for ethylene and pyrrole hydrogenation," *Journal of the American Chemical Society*, vol. 131, pp. 5816–5822, 4 2009. [Online]. Available: https://pubs.acs.org/doi/full/10.1021/ja809936n

[43] M. H. Hussain, N. F. A. Bakar, A. N. Mustapa, K. F. Low, N. H. Othman, and F. Adam, "Synthesis of various size gold nanoparticles by chemical reduction method with different solvent polarity," *Nanoscale Research Letters*, vol. 15, pp. 1–10, 7 2020. [Online]. Available: https://nanoscalereslett.springeropen.com/articles/10.1186/s11671-020-03370-5

[44] M. O. Olagunju, X. Poole, P. Blackwelder, M. P. Thomas, B. S. Guiton, D. Shukla, J. L. Cohn, B. Surnar, S. Dhar, E. M. Zahran, L. G. Bachas, and M. R. Knecht, "Size-controlled srtio3 nanoparticles photodecorated with pd cocatalysts for photocatalytic organic dye degradation," *ACS Applied Nano Materials*, vol. 3, pp. 4904–4912, 5 2020. [Online]. Available: https://pubs.acs.org/doi/full/10.1021/acsanm.0c01086

[45] I. Khan, K. Saeed, I. Zekker, B. Zhang, A. H. Hendi, A. Ahmad, S. Ahmad, N. Zada, H. Ahmad, L. A. Shah, T. Shah, and I. Khan, "Review on methylene blue: Its properties, uses, toxicity and photodegradation," *Water 2022, Vol. 14, Page 242*, vol. 14, p. 242, 1 2022. [Online]. Available: https://www.mdpi.com/2073-4441/14/2/242/htmhttps://www.mdpi.com/2073-4441/14/2/242

[46] M. Janus, K. Zajac, C. Ehm, and D. Stephan, "Fast method for testing the photocatalytic performance of modified gypsum," *Catalysts 2019, Vol. 9, Page 693*, vol. 9, p. 693, 8 2019. [Online]. Available: https://www.mdpi.com/2073-4344/9/8/693/htmhttps://www.mdpi.com/2073-4344/9/8/693

[47] S. Su, I. Siretanu, D. V. D. Ende, B. Mei, G. Mul, F. Mugele, S. Su, I. Siretanu, D. V. D. Ende, F. Mugele, B. Mei, and G. Mul, "Facet-dependent surface charge and hydration of semiconducting nanoparticles at variable ph," *Advanced Materials*, vol. 33, p. 2106229, 12 2021. [Online]. Available: https://onlinelibrary.wiley.com/doi/full/10.1002/adma.202106229https://onlinelibrary.wiley.com/doi/abs/10.1002/adma.202106229https://onlinelibrary.wiley.com/doi/10.1002/adma.202106229

[48] S. Zhu and D. Wang, "Photocatalysis: Basic principles, diverse forms of implementations and emerging scientific opportunities," *Advanced Energy Materials*, vol. 7, p. 1700841, 12 2017. [Online]. Available: https://onlinelibrary.wiley.com/doi/full/10.1002/aenm.201700841https://onlinelibrary.wiley.com/doi/abs/10.1002/aenm.201700841https://onlinelibrary.wiley.com/doi/10.1002/aenm.201700841

[49] Y. Fan, Y. Liu, H. Cui, W. Wang, Q. Shang, X. Shi, G. Cui, and B. Tang, "Photocatalytic overall water splitting by srtio3 with surface oxygen vacancies," *Nanomaterials*, vol. 10, pp. 1–10, 12 2020. [Online]. Available: /pmc/articles/PMC7767457//pmc/articles/PMC7767457/?report=abstracthttps://www.ncbi.nlm.nih.gov/pmc/articles/PMC7767457/

[50] E. P. Melián, O. G. Díaz, A. O. Méndez, C. R. López, M. N. Suárez, J. M. Rodríguez, J. A. Navío, D. F. Hevia, and J. P. Peña, "Efficient and affordable hydrogen production by water photo-splitting using tio2-based photocatalysts," *International Journal of Hydrogen Energy*, vol. 38, pp. 2144–2155, 2 2013.

[51] N. Fajrina and M. Tahir, "A critical review in strategies to improve photocatalytic water splitting towards hydrogen production," *International Journal of Hydrogen Energy*, vol. 44, pp. 540–577, 1 2019.

[52] S. Ye, R. Wang, M. Z. Wu, and Y. P. Yuan, "A review on g-c3n4 for photocatalytic water splitting and co2 reduction," *Applied Surface Science*, vol. 358, pp. 15–27, 12 2015.

[53] J. H. Kim and J. S. Lee, "Bivo4-based heterostructured photocatalysts for solar water splitting: A review," *Energy and Environment Focus*, vol. 3, pp. 339–353, 10 2014.

[54] L. Zhang, G. Tan, S. Wei, H. Ren, A. Xia, and Y. Luo, "Microwave hydrothermal synthesis and photocatalytic properties of tio 2/bivo4 composite photocatalysts," *Ceramics International*, vol. 39, pp. 8597–8604, 12 2013.

[55] A. Malathi, J. Madhavan, M. Ashokkumar, and P. Arunachalam, "A review on bivo4 photocatalyst: Activity enhancement methods for solar photocatalytic applications," *Applied Catalysis A: General*, vol. 555, pp. 47–74, 4 2018.

[56] P. S. Konstas, I. Konstantinou, D. Petrakis, and T. Albanis, "Development of srtio3 photocatalysts with visible light response using amino acids as dopant sources for the degradation of organic pollutants in aqueous systems," *Catalysts 2018, Vol. 8, Page 528*, vol. 8, p. 528, 11 2018. [Online]. Available: https://www.mdpi.com/2073-4344/8/11/528/htmhttps://www.mdpi.com/2073-4344/8/11/528

[57] B. Moss, Q. Wang, K. T. Butler, R. Grau-Crespo, S. Selim, A. Regoutz, T. Hisatomi, R. Godin, D. J. Payne, A. Kafizas, K. Domen, L. Steier, and J. R. Durrant, "Linking in situ charge accumulation to electronic structure in doped srtio3 reveals design principles for hydrogen-evolving photocatalysts," *Nature Materials 2021 20:4*, vol. 20, pp. 511–517, 1 2021. [Online]. Available: https://www.nature.com/articles/s41563-020-00868-2

[58] S. Patial, V. Hasija, P. Raizada, P. Singh, A. A. P. K. Singh, and A. M. Asiri, "Tunable photocatalytic activity of srtio3 for water splitting: Strategies and future scenario," *Journal of Environmental Chemical Engineering*, vol. 8, p. 103791, 6 2020.

[59] V. Deshmukh, C. Ravikumar, M. A. Kumar, S. Ghotekar, A. N. Kumar, A. Jahagirdar, and H. A. Murthy, "Structure, morphology and electrochemical properties of srtio3 perovskite: Photocatalytic and supercapacitor applications," *Environmental Chemistry and Ecotoxicology*, vol. 3, pp. 241–248, 1 2021.

[60] P. L. Hsieh, G. Naresh, Y. S. Huang, C. W. Tsao, Y. J. Hsu, L. J. Chen, and M. H. Huang, "Shape-tunable srtio3 crystals revealing facet-dependent optical and photocatalytic properties," *Journal of Physical Chemistry C*, vol. 123, pp. 13 664–13 671, 6 2019. [Online]. Available: https://pubs.acs.org/doi/full/10.1021/acs.jpcc.9b02081

[61] J. Ran, J. Zhang, J. Yu, M. Jaroniec, and S. Z. Qiao, "Earth-abundant cocatalysts for semiconductor-based photocatalytic water splitting," *Chemical Society Reviews*, vol. 43, pp. 7787–7812, 10 2014. [Online]. Available: https://pubs-rsc-org.ezproxy2.utwente.nl/en/content/articlehtml/2014/cs/c3cs60425jhttps://pubs-rsc-org.ezproxy2.utwente.nl/en/content/articlelanding/2014/cs/c3cs60425j

[62] G. Panomsuwan, N. Zettsu, and N. Saito, "Gold nanoparticles supported on srtio3 by solution plasma sputter deposition for enhancing uv- and visible-light photocatalytic efficiency," *Materials Research Society Symposium Proceedings*, vol. 1509, pp. 80–85, 2013. [Online]. Available: https://www.researchgate.net/publication/263237830_Gold_Nanoparticles_Supported_on_SrTiO3_by_Solution_Plasma_Sputter_Deposition_for_Enhancing_UV-_and_Visible-light_Photocatalytic_Efficiency_Gasidit

[63] M. F. R. Samsudin, L. T. Siang, S. Sufian, R. Bashiri, N. M. Mohamed, and R. M. Ramli, "Exploring the role of electron-hole scavengers on optimizing the photocatalytic performance of bivo4," *Materials Today: Proceedings*, vol. 5, pp. 21 703–21 709, 2018.

[64] B. Derjaguin and L. Landau, "Theory of the stability of strongly charged lyophobic sols and of the adhesion of strongly charged particles in solutions of electrolytes," *Progress in Surface Science*, vol. 43, pp. 30–59, 5 1993.

[65] E. J. Verwey, "Theory of the stability of lyophobic colloids," *The Journal of physical and colloid chemistry*, vol. 51, pp. 631–636, 1947. [Online]. Available: https://pubmed.ncbi.nlm.nih.gov/20238663/

[66] J. Adair, E. Suvaci, and J. Sindel, "Surface and colloid chemistry," *Encyclopedia of Materials: Science and Technology*, pp. 1–10, 1 2001.

[67] M. E. Labib, "The origin of the surface charge on particles suspended in organic liquids," *Colloids and Surfaces*, vol. 29, pp. 293–304, 1 1988.

[68] J. Israelachvili, "Intermolecular and surface forces," *Intermolecular and Surface Forces*, 2011. [Online]. Available: http://www.sciencedirect.com:5070/book/9780123751829/intermolecular-and-surface-forces

[69] L. Dong, H. Shi, K. Cheng, Q. Wang, W. Weng, and W. Han, "Shape-controlled growth of srtio3 polyhedral submicro/nanocrystals," *Nano Research 2014 7:9*, vol. 7, pp. 1311–1318, 8 2014. [Online]. Available: https://link.springer.com/article/10.1007/s12274-014-0495-y

[70] Y. Feng, S. R. Kilker, and Y. Lee, "Surface charge (zeta-potential) of nanoencapsulated food ingredients," *Characterization of Nanoencapsulated Food Ingredients*, pp. 213–241, 1 2020.

[71] A. Houas, H. Lachheb, M. Ksibi, E. Elaloui, C. Guillard, and J. M. Herrmann, "Photocatalytic degradation pathway of methylene blue in water," *Applied Catalysis B: Environmental*, vol. 31, pp. 145–157, 5 2001.

[72] M. Panalytical, "Mixed measurement mode phase analysis m3-pals for ease of use in zeta determination," 2010. [Online]. Available: https://www.malvernpanalytical.com/en/learn/knowledge-center/application-notes/an101104zetapotentialm3-pals

[73] K. Akhtar, S. A. Khan, S. B. Khan, and A. M. Asiri, "Scanning electron microscopy: Principle and applications in nanomaterials characterization," *Handbook of Materials Characterization*, pp. 113–145, 9 2018. [Online]. Available: https://link.springer.com/chapter/10.1007/978-3-319-92955-2_4

[74] J. Tschirch, R. Dillert, and D. Bahnemann, "Photocatalytic degradation of methylene blue on fixed powder layers: Which limitations are to be considered?" *Journal of Advanced Oxidation Technologies*, vol. 11, pp. 193–198, 7 2008. [Online]. Available: https://www.degruyter.com/document/doi/10.1515/jaots-2008-0202/html

[75] A. Aimable, A. Delomenie, M. Cerbelaud, A. Videcoq, T. Chartier, F. Boutenel, T. Cutard, and G. Dusserre, "An experimental and simulation study of heteroaggregation in a binary mixture of alumina and silica colloids," *Colloids and Surfaces A: Physicochemical and Engineering Aspects*, vol. 605, p. 125350, 11 2020.

[76] H.-J. Butt, K. K. Graf, and M. Kappl, "Physics and chemistry of interfaces," p. 361, 2003. [Online]. Available: https://www.wiley.com/en-us/Physics+and+Chemistry+of+Interfaces-p-9783527606405

[77] L. Sun, Z. Zhang, S. Wang, J. Zhang, H. Li, L. Ren, J. Weng, and Q. Zhang, "Effect of ph on the interaction of gold nanoparticles with dna and application in the detection of human p53 gene mutation," *Nanoscale Research Letters*, vol. 4, p. 216, 3 2009. [Online]. Available: /pmc/articles/PMC2894134//pmc/articles/PMC2894134/?report=abstracthttps://www.ncbi.nlm.nih.gov/pmc/articles/PMC2894134/

[78] Z. Su, F. Fang, S. Liu, N. Wang, Y. Wan, D. Guo, W. Han, and K. Chang, "Size-dependent al-doped srtio3 affecting solar-driven overall water splitting," *Catalysis Science Technology*, vol. 12, pp. 5003–5008, 8 2022. [Online]. Available: https://pubs.rsc.org/en/content/articlehtml/2022/cy/d2cy01146hhttps://pubs.rsc.org/en/content/articlelanding/2022/cy/d2cy01146h

[79] W. B. Russel, D. A. Saville, and W. R. Schowalter, *Colloidal dispersions*. Cambridge University Press, 1989.

[80] S. MASUYAMA, K. HORIKAWA, and S. YASUHARA, "The thermal decomposition products of citric acid added into the vegetable oils and their effect on the stability," *Journal of Japan Oil Chemists' Society*, vol. 13, pp. 533–537, 10 1964.

[81] M. G. Pamato, I. G. Wood, D. P. Dobson, S. A. Hunt, and L. Vočadlo, "The thermal expansion of gold: point defect concentrations and pre-melting in a face-centred cubic metal," *Journal of Applied Crystallography*, vol. 51, pp. 470–480, 4 2018. [Online]. Available: /pmc/articles/PMC5884389//pmc/articles/PMC5884389/?report=abstracthttps://www.ncbi.nlm.nih.gov/pmc/articles/PMC5884389/

[82] "Srtio3 heat capacity, melting point, density: Datasheet from landolt-börnstein - group iii condensed matter · volume 41e: "ternary compounds, organic semiconductors" in springermaterials (https://doi.org/10.1007/10717201_531)," copyright 2000 Springer-Verlag Berlin Heidelberg. [Online]. Available: https://materials.springer.com/lb/docs/sm_lbs_978-3-540-31362-5_531

[83] Y. M. Reddy, M. K. Nagaraj, S. S. Naik, and V. R. Reddy, "Annealing effects on electrical properties and interfacial reactions of ni/cu schottky rectifiers on n-type inp," *Journal of Modern Physics*, vol. 2012, pp. 538–545, 7 2012. [Online]. Available: http://www.scirp.org/journal/PaperInformation.aspx?PaperID=21098http://www.SciRP.org/journal/jmp

[84] L. Liu, P. Li, B. Adisak, S. Ouyang, N. Umezawa, J. Ye, R. Kodiyath, T. Tanabe, G. V. Ramesh, S. Ueda, and H. Abe, "Gold photosensitized srtio3 for visible-light water oxidation induced by au interband transitions," *Journal of Materials Chemistry A*, vol. 2, pp. 9875–9882, 6 2014. [Online]. Available: https://pubs.rsc.org/en/content/articlehtml/2014/ta/c4ta01988ahttps://pubs.rsc.org/en/content/articlelanding/2014/ta/c4ta01988a

[85] V. Iliev, D. Tomova, L. Bilyarska, and G. Tyuliev, "Influence of the size of gold nanoparticles deposited on tio2 upon the photocatalytic destruction of oxalic acid," *Journal of Molecular Catalysis A: Chemical*, vol. 263, pp. 32–38, 2 2007.

[86] Y. Guo, I. Siretanu, Y. Zhang, B. Mei, X. Li, F. Mugele, H. Huang, and G. Mul, "ph-dependence in facet-selective photo-deposition of metals and metal oxides on semiconductor particles," *Journal of Materials Chemistry A*, vol. 6, pp. 7500–7508, 5 2018. [Online]. Available: https://pubs.rsc.org/en/content/articlehtml/2018/ta/c8ta00781khttps://pubs.rsc.org/en/content/articlelanding/2018/ta/c8ta00781k

[87] L. F. D. Silva, O. F. Lopes, V. R. D. Mendonça, K. T. Carvalho, E. Longo, C. Ribeiro, and V. R. Mastelaro, "An understanding of the photocatalytic properties and pollutant degradation mechanism of srtio3 nanoparticles," *Photochemistry and Photobiology*, vol. 92, pp. 371–378, 5 2016. [Online]. Available: https://www.

researchgate.net/publication/299414871_An_Understanding_of_the_Photocatalytic_Properties_and_Pollutant_Degradation_Mechanism_of_SrTiO3_Nanoparticles

A Appendix

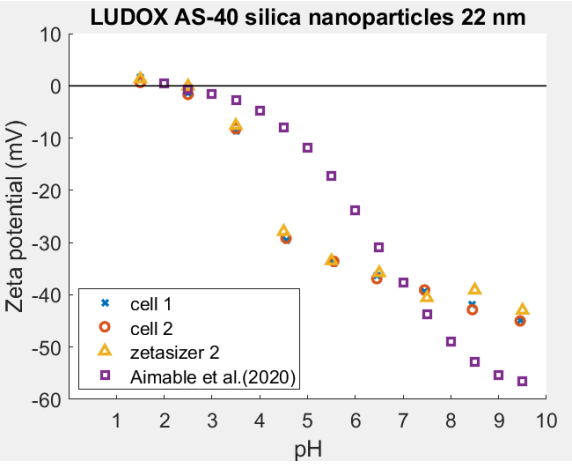

Figure 30: Plot of zeta potential as function of pH for different measurements of Ludox AS-40 silica nanoparticles with 22 nm size. Different measurements were done with different disposable cells and different Zetasizers and compared to measurements by Aimable et al. (2020) [75]

Matlab code is included, which was used to find the average distance between particles on a facet.

```
clear all
close all
clc
% 10 mM NaCl
A = imread('SB_BOX2_220620_108.tif');
B = imread('SB_BOX2_220620_108.tif');
B(1:1400,:) = [];% +- 2 pixels 169 pixels = 100 nm
A(1380:end,:) = [];
B(:,400:end) = [];%
B(:,1:20) = [];%20 to 400
B(130:136,:) = [];
B = B >= 250;
Bar = B(68,:);
Bar = nnz(~Bar); % 140 pixels -2 = 138 pixels -> 200 nm
scale = 100/138; % nm/pixels
LL  = A;
LL(250:420,460:660) = 0;
```

```
A = A(250:420,460:660); %640-780
DD = adapthisteq(A);
BW = DD >= 245;
BW = imrotate(BW,10);
A = imrotate(A,10);
BW(:,1:20) = [];
A(:,1:20) = [];
se = strel('disk', 3);
BW = imdilate(BW,se);
se2 = strel('disk',1);
BW = imerode(BW,se2);
stats = regionprops('table',BW,'Centroid',...
    'MajorAxisLength','MinorAxisLength');
centers = stats.Centroid;
diameters = mean([stats.MajorAxisLength stats.MinorAxisLength],2)
   ;
radii = diameters/2;
C = find(diameters<5);
centers(C,:) = [];
diameters(C,:) = [];
for i = 1:length(centers);
    for ii = 1:length(diameters);
        len(i,ii) = sqrt((centers(i,1) -centers(ii,1))^2+(centers
           (i,2)-centers(ii,2))^2); %length between each point
    end
end
dist = zeros(1,23);
for i = 1:length(centers);
    len(i,i) = 1000;
    dist(i) = min(len(i,:))*scale; %find minimum distance between
        each other particle
end
size = zeros(23);
avgdist = mean(dist); % 26 nm
size = scale*diameters;
avgsize = mean(size)

figure(2)
imshow(A)

figure(3)
```

```
56 hold on
57 imshow(BW)
58 % viscircles(centers,diameters);
59 hold off
60 figure(1)
61 hold on
62 imshow(A)
63 viscircles(centers,diameters);
64 hold off
65
66 figure(5)
67 imshow(LL)
```

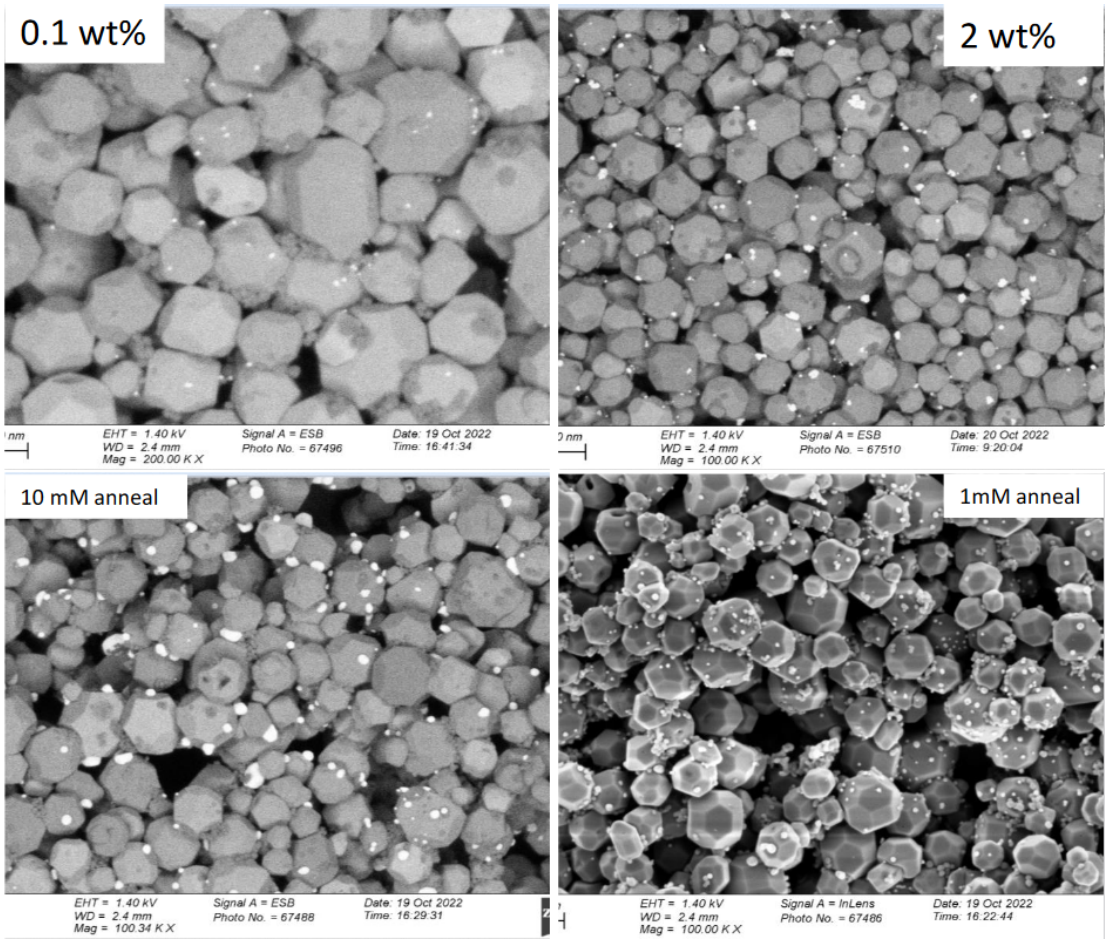

Figure 31: SEM pictures of $SrTiO_3$ with different ways of gold deposition before dye degradation. Top left: Photodeposition with 0.1 wt% of $HAuCl_4$. Top right: Photodeposition with 2 wt% of $HAuCl_4$. Bottom left: gold nanoparticle deposition at pH3, 10 mM NaCl, after annealing. Bottom right: gold nanoparticle deposition at pH 3, 1 mM NaCl, after annealing.

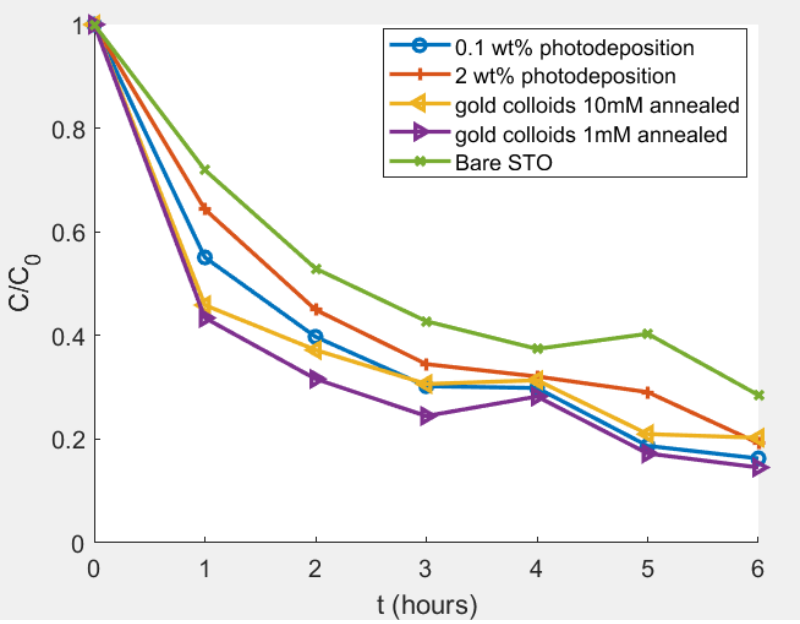

Figure 32: Graph of normalised concentration of Methylene Blue as function of illumination time. For this the same particles were used as in figure 31

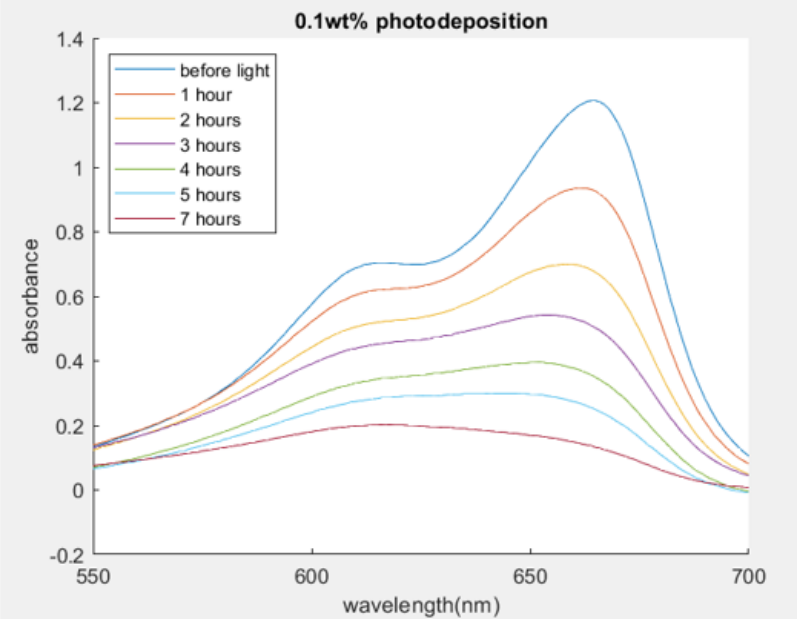

Figure 33: Absorbance spectrum of methylene blue dye over time, while being degraded by $SrTiO_3$ particles with 0.1 wt% photodeposited gold.